Study on Multipacting Phenomena of Low Temperature Cavity with respect to Condensed Gases on its Surface

A Dissertation Submitted to
the Department of Accelerator Science,
School of Mathematical and Physical Science,
Graduate University for Advanced Studies, Japan
as a Partial Fulfillment of the Requirements for the Degree of
Doctor of Philosophy

Md. Mashiur Rahman
2003

A Ph. D. Thesis

Study on Multipacting Phenomena of Low Temperature Cavity with respect to Condensed Gases on its Surface

By
Md. Mashiur Rahman

To

Prof. Shin-ichi Kurokawa

KEK & Graduate University for Advanced Studies, Japan

For his inspirational personality which has enrooted enthusiasm for the accelerator science and technology in my heart.

Acknowledgement

All praise to almighty Allah Whose infinite blessing enables me to be in that group of peoples who devote themselves to understand the boundless beauty of His noble creation - the whole universe. My gratitude is to the last prophet Hazrat Muhammad (peace be upon him), who has illustrated the way of Allah.

I would like to express my deep gratitude to Prof. Kenji Hosoyama of KEK for accepting me as his graduate student. Before joining his Crab cavity group, I have little exposure in experimental physics. He has taught me how an experiment can be arranged from the grass root level. He has enrooted the spirit and charm of experimental physics in my heart. His encouragement and all time smiling behavior have always eased me to pass my hard times during this work. I am very much grateful for his support and effort for successful completion of this work. I would like to remember his help in analytic calculation of rf field of our designed cavity and his illustration of electron trajectory in coaxial cavity by developing computer code. It is impossible to express in words my praise of his support during last couple of months when I was struggling with the pace of time. Without his help and suggestion, it was impossible to complete this work in time. I also convey my thanks to him for his valuable comments and corrections in writing this thesis. I will try to keep alive his sprit of experimental works in my career.

Prof. Shin-ichi Kurokawa of KEK - is the great man to whom I am in debt of sincere gratitude for my career in the field of high energy accelerator. It is he who has given me the opportunity to conduct my graduate research at the renowned organization KEK and thus introduced me the science and technology of high energy accelerator. I would like to remember his enthusiasm to introduce me the science and technology of high energy accelerator by arranging visit with him at Super-Kamiokande Neutrino detector, Gifu-ken, Japan and at JSPS Asian Science Seminar 2002 on Synchrotron Radiation Science, Jordan. Not only that, he has kindly spared more than 150 hours to teach me the physics of high energy accelerator. In these classes, his explanation and art of thinking was so captivating that my hungry for his next class will remain forever. In spite of hectic schedule, he has always taken care of my research work. I cannot refrain myself to mention that how emotional endowed in respect I have become by receiving his corrections and comments

on Chpater-3 of this thesis within a few hours in a late night. Indeed, it is his fatherly supervise and affection which have enabled me to complete this thesis in time. He will be always honored as a founder and inspirational person of my accelerator career.

Now I would like to pay my deep respect to Mr. Y. Kojima, Crab cavity group, KEK. His cooperation and participation in my research is unforgettable. By my heart, I am forced to remember an incident here. During setup of my cavity into cryostat, I surprisingly found that stainless steel sheets of radiation shield were of the same diameter as of the cryostat and so; cavity could not be placed into the cryostat. It was happened when my schedule was very tight and delicate. Situation was so terrible that I could not helped but looked for Mr. Kojima at 8 O'clock in night. Fortunately, I found this amiable person and not surprised to see his lovely smile after three hours hard labor to fix the problem. It is difficult for me to frame the praise of this kind of spontaneous support in linguistic words. I have learnt not only many experimental techniques and skills from this gentle man but also Japanese language. And coffee time with him will remain as one of the most memorable moments.

Here I would like to express my appreciation of enormous support of all other members of Crab cavity group. My sincere gratitude is to Mr. A. Kabe, particularly for his cooperation in computerization of my measurement system and also for introducing me with the rf measurement. Argon wielding is an essential part of my experimental setup and this demands the high appreciation of Mr. K. Hara's skill. My thanks also wave to Mr. Yatabe for producing liquid Helium in pace of my schedule. I am in great debt of gratitude to Dr. H. Nakai, who has helped me from the very beginning. By his kindness, he took all the responsibilities of dealing a lot of official affair, both academic and non-academic. I am also indebted to him for his effort in fixing the ghostly problems with my Apple computer. I gratefully remember the impressive discussions with Dr. Y. Morita. My warmest regard is to Mr. K. Nakanishi, a graduate student of my supervisor. I had to use his computers to arrange my thesis book in this present format.

I convey my thanks to all scientists and staffs of KEK for their eager to help on request. I am very much grateful to Prof. Masanori Kobayashi for his impressive lectures on Vacuum Science and Technology and also for his keen interest and discussion on our experiments. I also express my gratitude to Prof. Toshio Kasuga for his lectures on RF Fundamentals and discussion on multipacting experiments. I would like to also remember the discussion with Prof. Shinji Mitsunobu and Prof. Takaaki Furuya. My admiration is to Ms. Yoko Hayashi for her sincere cooperation. I also appreciate all the people of Hitachi Retouki Group, particularly Mr. T. Kanekiyo and Mr. K. Isa for their spontaneous help. I also would like to express my gratitude to the Government of Japan for the support of my education here.

Now I would like to express my warmest thanks to Dr. M. Khaliquzzaman, Chief Scientific Officer (retd.), then Head of Physics and Material Science Division, Bangladesh Atomic

Energy Commission (BAEC), Bangladesh and Dr. C. S. Karim, Member of Physical Science, BAEC. Without their help, it was almost impossible to come KEK by crossing a lot of hurdles. I also remember the great support offered by my then BAEC colleagues Dr. S. K. Biswas, Chief Scientific Officer, Chemistry Division and Mr. Md. S. Islam, Scientific Officer, NDT Division.

Among the non-academic people, I would like to express my gratitude to wife of Prof. Shin-ichi Kurokawa for her cordiality to my family. I cannot express in words my admiration of her letter to me, which was full of inspiration and affection. I also respectfully remember the hours shared between my supervisor Prof. Kenji Hosoyama's family and my family. I am also grateful to Dr. H. Nakai's family for their warm company during my first two years lonely life.

To my respected parents, I owe more than I can express in words, for their constant inspiration in learning from my childhood. It is their motivation by which I have chosen my career in R&D. I also convey my deep respect and gratitude to my parents-in-law for their keen interest and inspiration in my research career. I would like to appreciate encouragement and support of my sweet wife Urmi who never showed any short of discontent although she had to stay alone all the day and even sometimes for the whole night in a single room apartment for months after months. I also respectfully remember my younger brothers Lotus and Titus and my only one sweet sister Nadira for their boundless support to my success.

May all-kind Allah enable me to build up my career as a renowned accelerator scientist.

Abstract

Multipacting is a common phenomenon of spontaneous electron loading in resonant structures, either normal or super conducting. These electrons interact with the rf field inside the resonant structure and thus cause an abrupt and huge loss of rf field. As a result, multipacting appears as a performance limiting phenomenon of resonant structures, e.g., cavity and waveguide.

In the case of superconducting cavity, due to cool down to cryogenic temperature from room temperature, residual gas molecules adsorb on the inner surface of cavities and couplers. A common speculation is that these adsorbed molecules enhance the multipacting. In the research and development of superconducting Crab cavity for KEKB electron-positron collider, a severe multipacting is observed during the first time rf excitation after the cool down at 4.2K from room temperature. After processing the multipacting, if the cavity is kept at 4.2K, this multipacting is never observed during the following rf excitation. Also, in the case of KEKB superconducting accelerating cavities, multipacting is observed at and around the input coupler during the long time operation of KEKB. This observance of multipacting may be explained as that adsorption of residual gas molecules may cause this multipacting. Being inspired by these experimental hints, we have devoted our effort to understand the multipacting with respect to the adsorbed gas molecules.

Our study is different from the present trend of multipacting research — simulation of multipacting and study on secondary yield. In our study, we have focused our concentration in the origin of multipacting. What molecules are responsible in multipacting? Is there any difference between monolayer and multilayer of adsorbed molecules in multipacting? In our study, we have tried to find out this kind of fundamental answers in an attempt to trace out the seed of multipacting.

At first, we have designed and built up a dedicated experimental setup to learn the adsorption and desorption of residual gas molecules on cryo-cooled surface. Most exciting part of our experimental setup is to develop a Gas Flow Control System, by which we have efficiently controlled the number of molecules admitted into the vacuum chamber. This has enabled us to study the adsorption and desorption of gas molecules with respect to mono-

layer and multilayer. As the experimental surface on which adsorption and desorption has been studied, we have designed a cylindrical vacuum chamber. This vacuum chamber has been fabricated from the thick cylindrical pipe of oxygen free high conductivity (OFHC) copper so that the temperature distribution along the length of vacuum chamber becomes negligible. Since the most dominant residual gas molecule in ultra high vacuum is H_2, we have extensively studied the adsorption and desorption of H_2. We have found that H_2 has a saturated pressure of the order of 10^{-4} Pa at 4.2K. Desoprtion of H_2 from monolayer as a function of temperature can be characterized by a broad peak at 14K. On the contrary, desorption of H_2 from multilayer occurs very sharply at around 5.6K.

Experience of the adsorption desorption experiment has been carried in the experiment of multipacting with respect to adsorbed gas molecules. For this study, we have designed and built up a coaxial type resonant cavity of resonant frequency is 1.5 GHz. Mode of excitation has been so chosen that different cutting parts, for example, vacuum opening at inner conductor, have been adopted at the places where rf surface current is zero. This mode selection has enabled us to build up a coaxial cavity of rather high unloaded Q_0 from OFHC copper. Another important feature of our design is that the inner and outer conductor can be easily separated from each other. This feature provides different options to study the multipacting. For example, besides the very easy access to the multipacting site, we can change the surface condition at the probable multipacting site. We have also designed and built up the unit coupling input probe, different monitor probes and the cryostat top flange.

To study the multipacting, we have used three parameters: i) vacuum pressure, particularly, for multipacting at room temperature, ii) current due to multipacting electrons, and iii) reflected and transmitted signals from the cavity. In the study of room temperature multipacting, We have found that after processing of the multipacting observed below the peak electric field of 0.28 MV/m, these multipacting incidents do not occur during the subsequent rf excitations, if the cavity is not exposed to ambient air. Multipacting above the peak electric field of 0.28 MV/m occurs during every rf excitation, even if the cavity is not exposed to ambient air. Room temperature multipacting observed above 0.3 MV/m has been found not to become processed without baking at 100^0C. This effect of baking hints that water molecule may cause or enhance multipacting. In contrast to room temperature, multipacting levels at 4.2K are few and soft. Once processed, multipacting does not occur if the cavity is kept at 4.2K. We have studied the multipacting at 4.2K with respect to different amount of adsorption of H_2 - from saturated H_2 surface to partial monolayer of H_2. Our experiment has revealed that adsorbed H_2 does not act as the seed of multipacting, rather suppresses the multipacting. We have also studied the effect of other dominant residual gas molecules CO. We have found that CO too does not act as the seed of multipacting. Also, the development of multipacting in microsecond level has been studied.

Contents

List of Figures

List of Tables

Chapter 1

Introduction

Main objective of this chapter is to explain the motivation of our study. Both experimental approach and objectives are also mentioned.

1.1 RF Cavity

Now-a-days, accelerator and its technology is not only important for the elementary particle physics, but also for the wide application in different applied researches such as material science, medical science, and molecular science. Radio frequency (rf) cavity is the heart of a modern particle accelerator. RF cavity is used to provide energy to the particle beam. Due to growing demand of both energy and luminosity, superconducting, particularly niobium, cavity becomes the indispensable source of particle energy in present day's accelerators. In very near future, superconducting rf cavity known as Crab cavity, will be used to deflect the beam in KEKB [1] electron-positron collider.

Due to various reasons, maximum accelerating gradient of superconducting cavity has been never reached up to the theoretical limit [2]. One of the reasons is the loss associated with the residual resistance. Impurity in the superconducting material itself, adsorbed gas molecules and trapped magnetic flux may be the main sources of residual resistance. Besides this loss, the other common losses are field emission, thermal breakdown and multipacting.

[1] KEKB is a one of the two electron-positron colliders dedicated for the CP violation study.

[2] This theoretical limit is due to the superheating magnetic field. For niobium, theoretical value of superheating magnetic filed is 240 mT at 0K [1]. This yields around 60 MV/m maximum accelerating gradient for niobium cavities.

At high field level, electrons come out from the microscopic defects on the cavity inner surface. These electrons are accelerated by the rf electric field and impact on the cavity wall. As a result, impact site becomes heated up and x-rays in the range 0.1 – 1 MeV is produced. This phenomenon is known as *field emission* and the defects are called field emitters. Due to field emission, an exponential drop in Q_0 as a function of peak electric field E_{pk} is observed. RF and He processing are applied to process the emitter but another emitter may appear at higher rf power. Detection of x-ray near the cryostat and scanning the temperature of cavity surface provides the powerful ways to detect the field emission and emitters. For a detailed picture of field emission, it may be very useful to go through the Ref. [2].

Thermal breakdown occurs when a large fraction of the cavity becomes normal conducting prematurely and as a result, abruptly a huge amount of stored energy is lost into Joule's heating. When the field inside the cavity becomes sufficiently small, cavity is cooled by the liquid He and thus regains the original condition. This whole process repeats and so reflected and transmitted signal from the cavity looks like saw-tooth wave. Thermal breakdown limits a sharp degradation of the quality Q_0 at a peak electric field. This anomalous loss is usually happened due to normal conducting particulates (e.g., inclusion of foreign material during welding, residuals from the cleaning process) strongly attached with the cavity inner surface and imperfections of the superconducting material itself. This also may happen due to impact of electrons generated from field emission and multipacting.

Multipacting is another anomalous loss due to electron impact. Since multipacting is of our main concern, it is discussed more elaborately in the next section.

1.2 Multipacting

Multipacting is a resonant phenomenon in which copious electrons are generated from the cavity inner surface within a very short time. These electrons interact with the rf field inside the cavity and thus extract stored energy of the cavity. This extraction of stored energy can be experimentally observed by following the transmitted signal from the cavity in oscilloscope. Figure 1.1 shows the time structure of the transmitted signal of a cavity driven by pulse power. Sometimes, the loss of stored energy due to multipacting electrons is so huge that it seems as if a barrier is present against the increase of the stored energy by raising the input rf power. As a result, an abrupt fall of the cavity quality as a function of peak electric field is observed experimentally. Indeed this situation was frequently happened before the use of present day's spherical or elliptical shaped cavity.

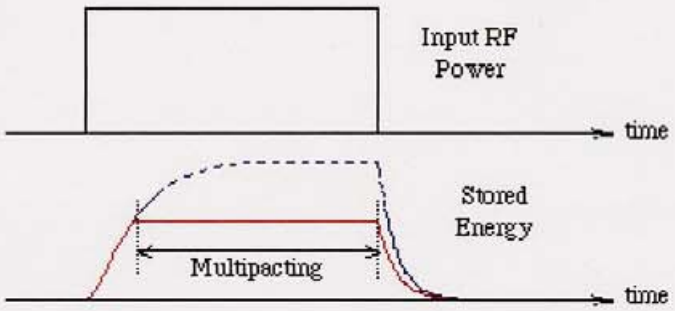

Figure 1.1: Due to Multipacting, change in time structure of stored energy of a cavity operated in pulse mode (dotted line (blue) - during Multipacting, solid line (red) - without multipacting).

Usually a multipacting barrier is surmounted by rf processing. This is done by allowing multipacting to progress for an interval of time while slowly raising the rf power. Eventually, and sometimes abruptly, multipacting ceases. Very often, further barriers appear at higher field levels. These may be processed as well. But sometimes this processing becomes impossible due to limitation of available input rf power.

Upon impact, multipacting electrons release heat on the cavity surface and thereby cause localized increase of the surface resistance. This increases the cavity losses. Sometimes, this localized heating even may cause thermal breakdown. But this localized heating enables us to detect the multipacting site.

1.2.1 Theory of Multipacting

Due to different reasons such as cosmic rays, photoemission and field emission, some electrons come out from the inner surface of the rf cavity. If one of these stray electrons is in favor of the rf field of the cavity, then the electron is accelerated and eventually impacts on the cavity wall. This impact results in a number of electrons known as secondary electrons. The number of secondary electrons depends on the impact energy and the condition of the surface. These secondary electrons are again accelerated and, upon impact, produce another generation of electrons. This process is continuing on. As a result, if the secondary electron emission coefficient is larger than one, there is an avalanche of electrons inside the cavity in a very short time, almost instantaneously. This is the mechanism of multipacting.

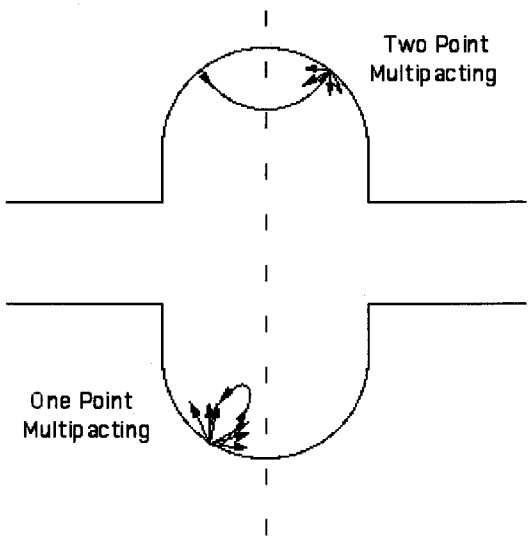

Figure 1.2: A very simplistic view of two common multipacting trajectories.

Trajectories of multipacting electrons are very complex. Depending on the closeness of emission and impact sites, there are two common types of trajectories, known as one point and two point multipacting.

In one point multipacting, secondary electrons impact the cavity wall at or very near to the emission site. But in case of two point multipacting, impact and emission sites are far away, usually involving two opposite rf surfaces. Obviously, to be accelerated, secondary electrons should be either in same phase (one point multipacting) or opposite phase (two point multipacting) relative to the primary electron. This reveals that multipacting is essentially a resonant phenomenon where time between the two consecutive impacts should be integer (one point multipacting) or half-integer (two point multipacting) multiple of rf time period. Number of rf periods elapsed in between the two consecutive impact with the cavity surface is referred as the order of multipacting. In addition to the resonant condition, secondary electron emission coefficient of larger than unity should be fulfilled to occur the multipacting.

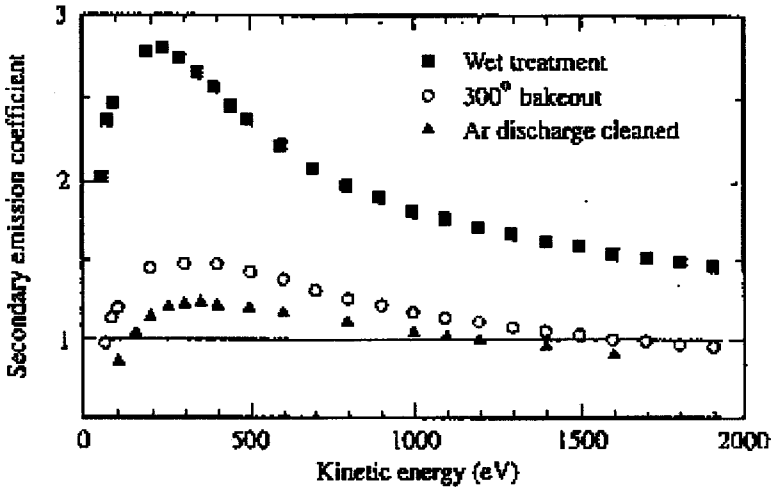

Figure 1.3: Secondary electron emission coefficient of a niobium surface after different surface treatment [2].

1.2.2 Secondary Electron Emission Coefficient

For most materials, the secondary electron emission coefficient is larger than unity for the impact energy in the range from a few tens of eV to a few thousands of eV. In this range, magnitude of the secondary electron emission coefficient varies significantly from material to material. However, the general behavior is similar to that shown in Figure 1.3.

Since secondary electron emission occurs at the surface, surface preparation is very important to control the secondary electron emission. This is also revealed out in the Figure 1.3. One of the steps of cavity preparation is wet treatment, which results in large secondary emission over the entire measured region of impact energies. Argon discharge cleaning or baking are very effective in reducing secondary electron emission.

Adsorbed particles also increase the secondary electron emission. Residual gas molecules, hydrocarbons from the pump oil and lubricants used in polyethylene [3] are the main sources of adsorbed particle.

1.3 Review of Multipacting Studies

Multipacting problem drew attention from the very early time of use of pill box shape rf cavity. At that time, many studies were carried out to understand this problem. For a brief review, one may go through the Ref. [4], [5] and [6]. It was found that field limitation in pill box type cavity was caused by the one-point multipacting. A remarkable solution to this one-point multipacting is to change the cavity shape into the spherical one. In this shape, electrons drift to the equator within a few impacts and so, no stable trajectories is possible. At the equator the electric field vanishes and so secondary electrons do not gain any energy. As a result, generation of secondary electrons stops very quickly and does not favor to resonant multipacting. Later elliptical shape cavity was developed and reported free from multipacting [7]. But these spherical and elliptical shape cavities are not completely free from multipacting. Two-point multipacting was reported to occur in these cavities [8], [9].

Problem of Multipacting is more severe in the case of coaxial structures, for example, input coupler and waveguides required to feed rf power to the cavities [10] – [12]. To understand the multipacting in this arena, and thereby, to find out the best suppression method, most of the present studies concentrate on the simulation of multipacting [13] – [15].

Another crucial factor of multipacting is the secondary electron emission coefficient. So, in past as well as present days, many studies have been carried on to determine the secondary electron emission coefficients and thus to find out the best way of preparation of cavity surface [3],[16] – [20].

1.4 Objective of our Study

In KEKB electron-positron collider, a superconducting cavity, well known as Crab Cavity will be used to realize the finite angle head-on collision. Figure 1.4 shows the conceptual design of the Crab cavity. This cavity is designed to deflect the beam transversely electrically. So, the mode TM_{110} rather than the fundamental mode TM_{010} is used. To extract the fundamental mode, a coaxial coupler is adopted. Without this coaxial coupler, there is not so much multipacting. But with the introduction of the coaxial part, a serious multipacting is observed. Multipacting observed in the Crab cavity with the coaxial coupler is illustrated in the Figure 1.5. When there is no multipacting, time structure of the reflected and transmitted signal from the cavity driven by rf pulse has the characteristic form as shown in the right-bottom part of Figure 1.5 (Here, the cavity was little bit over coupled.).

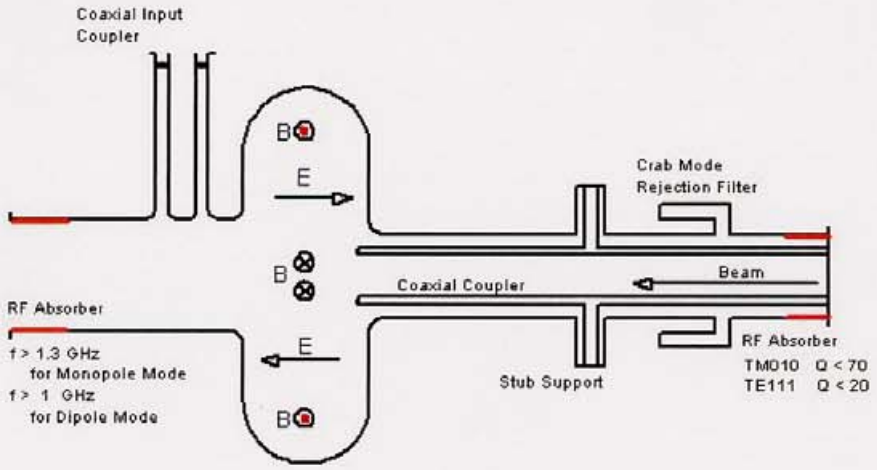

Figure 1.4: Conceptual design of KEKB Superconducting Crab cavity.

After cooling to 4.2K from room temperature, during the very first rf excitation, crab cavity with the coaxial coupler exhibited the time structure as shown in the upper-left part of the figure at low rf power (a few watts). Since power was too low for field emission, this time structure could be explained by the electron loading due to multipacting. As illustrated in the Figure 1.5, it took about one hour to rf process this multipacting. Once processed, this multipacting never occurred during the following rf excitation if the cavity was kept at liquid helium temperature. After warm up to room temperature, this multipacting was again observed during the very first rf excitation after cool down the cavity. This observance of multipacting led to the speculation that adsorption of residual gas molecules might cause this multipacting. Due to multipacting, adsorbed gas molecules desorb from the multipacting site and thus once processed, there is no reoccurrence of multipacting.

Also, during the long time operation of KEKB electron-positron collider, multipacting is observed at and around the input coupler of the superconducting accelerating cavities although the aging of input coupler is done before the operation. This observance may be explained by the adsorption of residual gas molecules on the surface of input coupler from the beam pipe. In order to desorb out the adsorbed gas molecules, rf processing with bias voltage is applied to the input coupler [10].

These experiences prompted us to study the multipacting in the coaxial structure with respect to the adsorbed gas molecules. In contrast to the present trend of multipacting research, we concentrated our devotion in the origin of multipacting. Which molecules are responsible in multipacting? Is there any difference between monolayer and multilayer of adsorbed gas molecules in occurring multipacting? In our study, we dedicated our effort to find out this kind of fundamental answers to trace out the seed of multipacting.

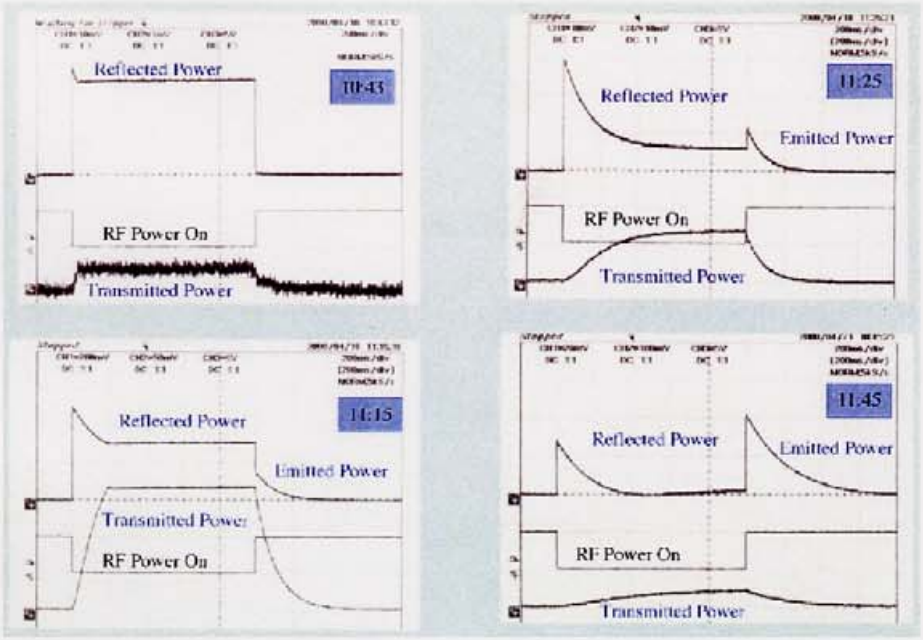

Figure 1.5: rf processing of multipacting observed in KEKB Crab cavity with the coaxial coupler.

1.5 Sketch of our Study

When the superconducting cavity or coupler is cooled at cryogenic temperature, residual gas molecules adsorb on the inner surface. There is a common speculation that these adsorbed molecules play a crucial role in multipacting. In order to study the adsorption and desorption of residual gas molecules, we designed and built up a dedicated experimental setup, named as Adsorption Desorption Experiment. We designed and built up all the parts of this experimental setup – starting from the pumping system to the computer based data acquisition system. The most important and difficult part was to develop a very simple system by which we efficiently controlled the admission of sample gas molecules into the vacuum chamber, whose inner surface served as the experimental surface for our adsorption and desorption experiment.

Along with this experiment, we designed and built up another set up to study the multipacting on copper surface regarding the adsorption of different residual gas molecules. Our experimental set up was designed to form monolayer or multilayer of the experimental gas molecules. This enabled us to study the behavior of multipacting with respect to the number of layer of the adsorbed gas molecules. A coaxial cavity was designed so that we can prepare localized modification of surface condition. This design feature allows us to study the effect of surface condition, especially surface roughness.

1.6 Organization of the Dissertation

As mentioned in the last section, we have built up two separate experimental setups, namely Adsorption Desorption Experiment and Multipacting Experiment. Chapter 2 describes the Adsorption Desorption Experiment in full depth starting from the experimental setup, experiments with H_2 gas molecules and results. Similarly, Chapter 3 describes the details of Multipacting Experiment. Chapter 4 summarizes our experimental findings.

Chapter 2

Adsorption Desorption Experiment

When a vacuum chamber e.g., cavity or coupler is cooled from the room temperature, residual gas molecules adsorb on the inner surface of the vacuum chamber. This adsorption occurs due to i) adhesive attraction force between the chamber surface material and the gas molecules, ii) adhesive force between the different gas molecules, and iii) cohesive force between the same gas molecules. How do the gas molecules desorb? Obviously energy larger than the adsorption energy is needed to desorb the gas molecules from the surface. But the complete picture may be not so simple because of the adsorption[1] of different molecules at different temperatures. Again, desorption of the same molecules from monolayer should be different from the multilayer. What is the difference? For a clear understanding of these phenomena, we devoted ourselves to build up the following dedicated experimental set up.

2.1 Experimental Set up

Figure 2.1 schematically shows the experimental setup of the Adsorption Desorption experiment. Besides the measurement system, this setup consisted of a vacuum chamber, pumping system, cryostat top flange and gas flow control system. Since our experiment should be carried on at cryogenic temperature, at first we had to think of cryostat. KEK Crab cavity group already had some cryostats of inner diameter 200 mm. Size of these cryostats were enough to fit our experimental purpose. So, in order to save the cost and time, we used one of these cryostats. Taking the dimension of this cryostat, we designed and built up all the other parts of the experiment.

[1]By adsorption we mean that case when adsorption time is comparable to the experimental time.

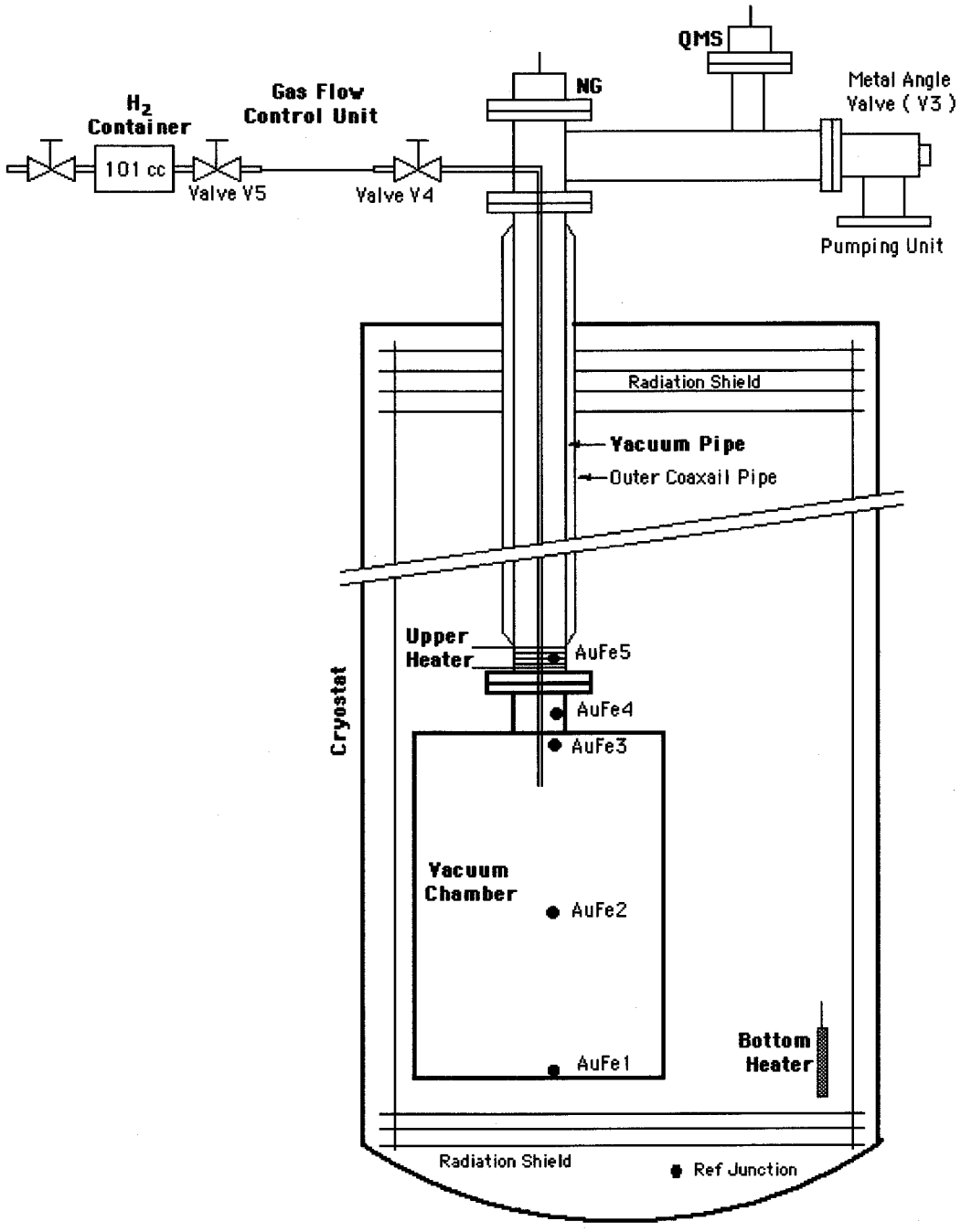

Figure 2.1: Schematic view of the experimental setup of Adsorption Desorption Experiment.

2.1.1 Pumping System

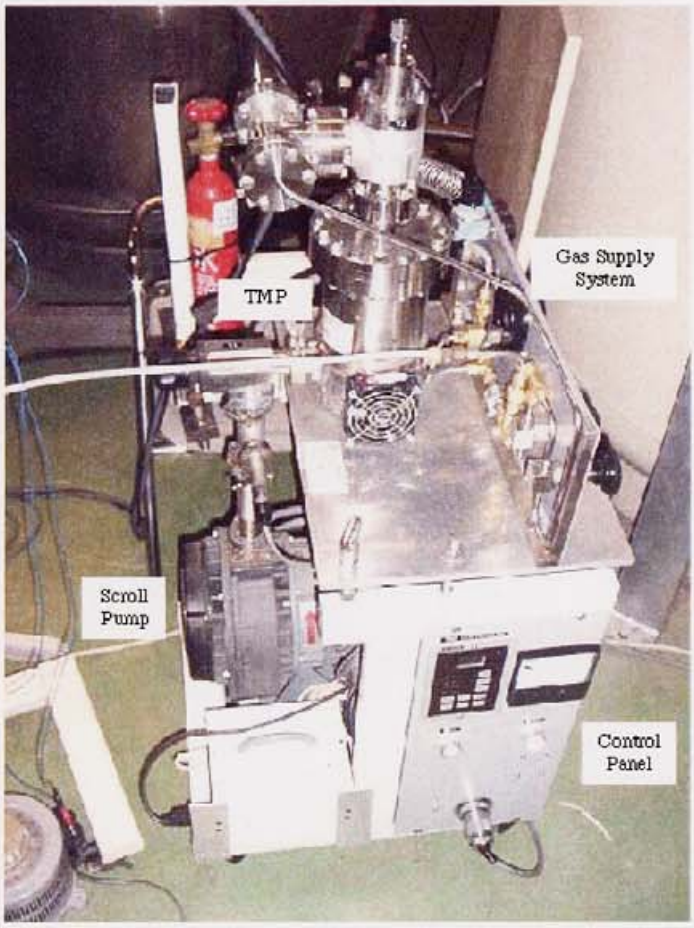

Figure 2.2: Oil free high vacuum pumping unit.

We built up an oil free pumping system to achieve a vacuum better than 10^{-6} Pa at room temperature. We used the oil free pumping system so that any oil molecules could not enter the vacuum chamber. Our pumping system was consisted of a turbo-molecular pump[2] backed by an oil free scroll pump[3]. Figure 2.2 shows the photograph of the pumping system.

In our experimental setup, we used Bayard-Alpert type Nude gauge to measure the total vacuum. Sometimes filament of this nude gauge becomes burnt out due to various reasons, for example, accidental leak. During the change of burnt filament, we admitted dry N_2 gas into the vacuum part of our setup so that the vacuum part did come into a minimum contact with the atmospheric wet air. To do this, our pumping system was equipped

[2]Model UTM-150, ULVAC designed for vacuum 10^{-8} Pa.
[3]Model ISP-250B, ANEST IWATA.

with a gas supply system. In our experiments, this gas supply system also was used to fill up the experimental gas (H_2 and CO) into a small container from the large high-pressurized container.

2.1.2 Cryostat Top Flange

In our experimental design, the most important part of the cryostat top flange was a vacuum pipe, which simultaneously served as the connecting pipe between pumping system and vacuum chamber and as the holder of the vacuum chamber into the cryostat. This vacuum pipe hung the vacuum chamber from the ceiling of top flange. In our experiment we wanted that adsorption of the experimental gas molecules took place only on the inner surface of the vacuum chamber. This required that temperature of the vacuum pipe should be fairly higher than the temperature of the vacuum chamber. For this purpose, the vacuum pipe was coaxially placed into another cylindrical pipe (illustrated as Outer Coaxial Pipe in Figure 2.1) and the annular space between these two pipes was maintained at vacuum of the order of 10^{-1} Pa at room temperature. This annular space acted as a temperature isolation space. Also, a heater, named upper heater, was wound around the lower end of the vacuum pipe just above the connecting flanges in order to prevent cooling by conduction. This heater (30 watt, 15V) was made from manganese wire of diameter 0.2 mm and resistance 15.16 Ω/m.

2.1.3 Vacuum Chamber

We designed a cylindrical vacuum chamber as the surface on which adsorption and desorption was studied. In order to keep the temperature distribution along the length of vacuum chamber minimum, we fabricated the vacuum chamber from a thick cylindrical pipe of oxygen free high conductivity (OFHC) copper. This OFHC copper pipe was made from cylindrical copper rod by extrusion. End plates were made of copper of thickness 7 mm. All parts were joined by vacuum silver brazing. Figure2.3 shows the photograph of the vacuum chamber. In this figure, outside surface of the vacuum chamber looks ash-black because of baking at 150^0C. Table 2.1 shows the dimensions and related parameters of the vacuum chamber.

Number (mentioned in Table 2.1) of H_2 molecules required to form the monolayer was calculated on the assumption that H_2 molecules were closely packed in a face-centered cubic lattice. Geometrical surface of a H_2 molecule is $(\sqrt{3}/2)\delta^2$, where $\delta = 2.75 \times 10^{-8}$ cm.

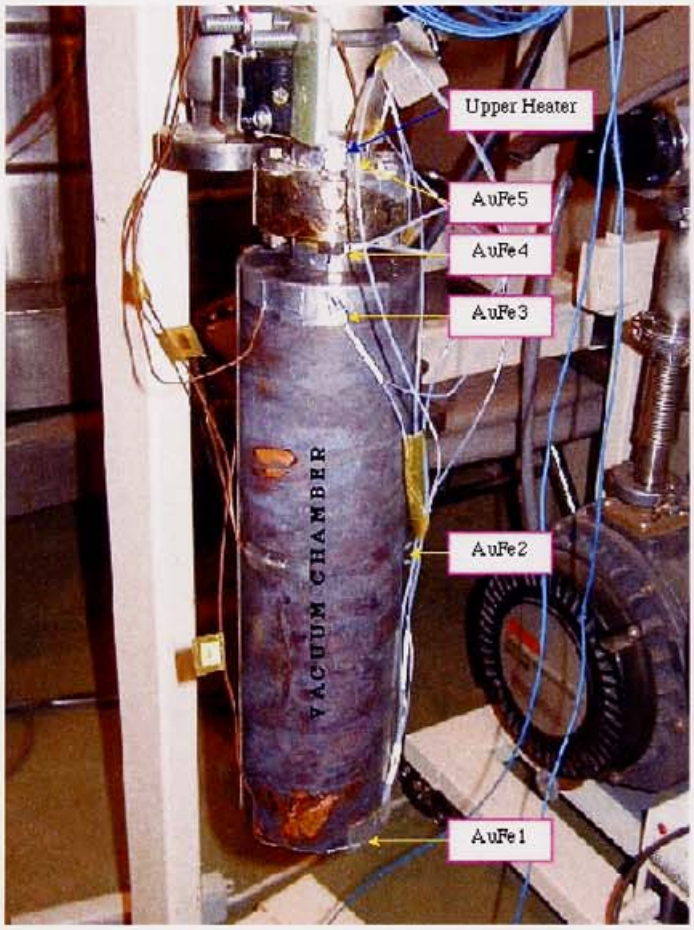

Figure 2.3: Photograph of our designed vacuum chamber. This photograph was taken after baking at 150^0C in ambient air. So, its outside surface turned ash color.

Table 2.1: Dimension of Vacuum Chamber

Parameter	Value
Outer Dimension	85 mm
Thickness	6.2 mm
Inner Length	300 mm
Inner surface	792.6 cm^2
No. of H_2 molecules to form a monolayer	1.21×10^{18}

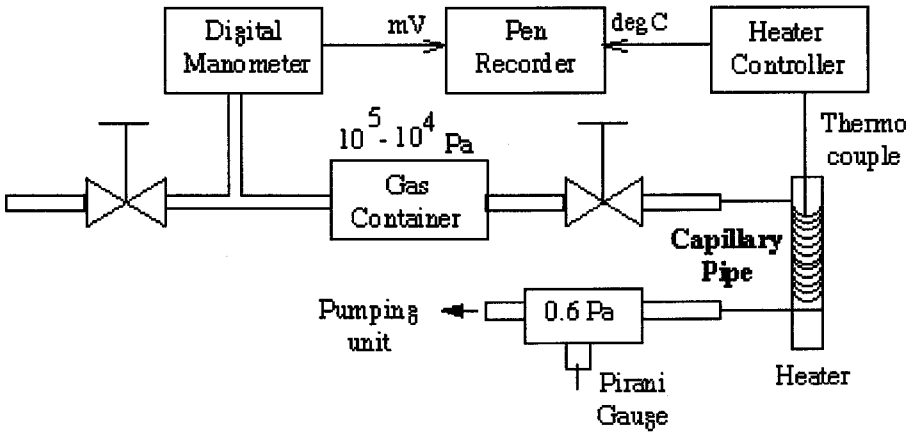

Figure 2.4: Schematic view of the flow rate measurement setup.

2.1.4 Gas Flow Control System

Since the dominant residual gas molecule at very high vacuum is hydrogen, we had decided to study, at first, the adsorption and desorption of hydrogen gas molecules. In order to form a monolayer of H_2 molecules on our vacuum chamber surface, we needed an order of 10^{18} molecules (Table 2.1). This number of molecules equivalents about 0.04 cc H_2 gas at standard temperature and pressure. To feed such a small amount of H_2 gas molecules into the vacuum chamber, a very slow gas supply system was required.

To develop such a slow supply system, we took a stainless steel capillary pipe of inner diameter of about 0.1mm. This was the thinnest capillary pipe commercially available. Since viscosity of gas increases with temperature, in first attempt, we studied the flow rate of H_2 gas through the capillary pipe as a function of temperature. Figure 2.4 shows the schematic view of the experimental setup of the flow rate measurement. Figure 2.5 shows the photograph of the real experimental setup. One meter long capillary pipe was wound on a cylindrical heater. At both ends of the capillary pipe, 50 mm long copper pipe of diameter 3.2 mm (1/8-inch) were joined by silver brazing to adopt the vacuum Swagelock nut (Figure 2.6). Then one end was connected with the sample gas (H_2) container and other end was connected with the dummy vacuum chamber. A T-type connector (and the long connecting pipe) between the capillary pipe and pumping unit was used as the dummy vacuum chamber. Vacuum pressure of the dummy chamber was measured by a pirani gauge mounted on the side arm of the T-type connector. Vacuum pressure of the dummy chamber was maintained at 0.6 Pa during the measurement. Pressure of the sample gas (H_2) container was measured by a digital manometer.

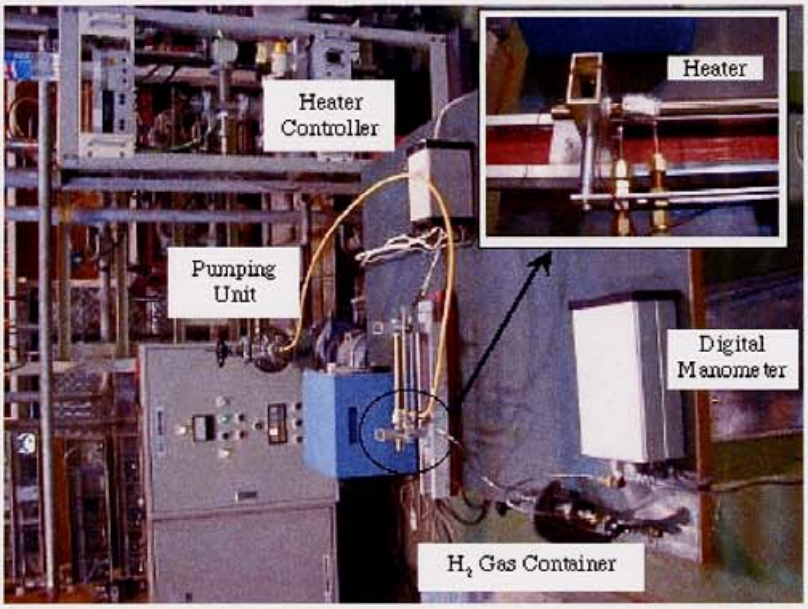

Figure 2.5: Photograph of the real setup of the flow rate measurement through the capillary pipe. Inset photograph shows the arrangement of the capillary pipe on a heater. Capillary pipe was wound around the heater and then covered with aluminum foil.

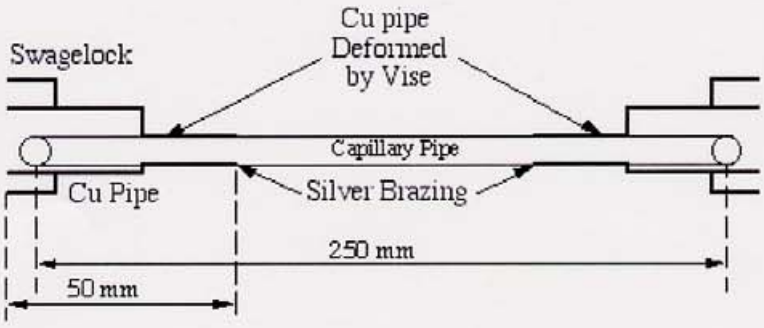

Figure 2.6: Schematic view of the joint of the capillary pipe with 1/8 inch Cu pipe.

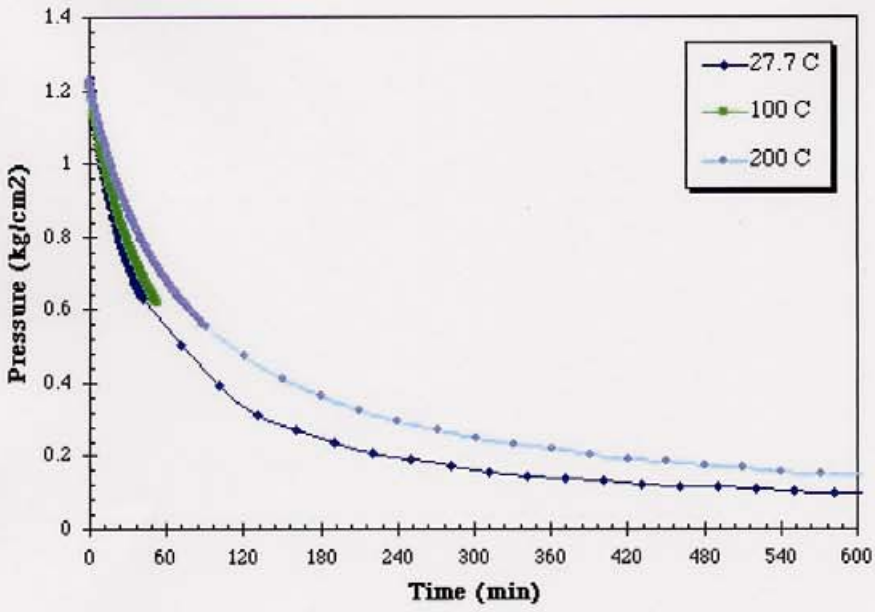

Figure 2.7: Flow rate of H_2 gas molecules through a 1m long capillary pipe at different temperatures.

Figure 2.7 shows the fall of pressure of the sample gas (H_2) container through the one meter long capillary pipe kept at different temperatures. Since pressure of the gas container is directly proportional to number of gas molecules, this fall of pressure also indicated the flow rate of H_2 gas molecules through the capillary. Obviously the flow rate decreased with temperature but the rate of decrease was very slow. For example, at pressure 0.15 kgf/cm^2, flow rate of H_2 gas molecules at 200 ^{0}C was 0.01 kgf/cm^2-hour, which was about two times slower than the flow rate at 27.7^{0}C.

Another idea, we studied, was to deform the capillary pipe along the cross-section. Obviously, this cross-sectional deformation increases the impedance to flow of gas molecules. We made a simple gadget, as shown in Figure 2.8, to make the deformation. Structure of the deformation is shown in Figure 2.9. Length of deformation was 5 mm and gap between successive deformations was 1 mm. Figure 2.10 shows the flow rate of H_2 gas molecules as a function of number of deformations through a 250 mm long capillary pipe. Compared to the method described in the preceding paragraph, cross-sectional deformation of the capillary pipe proved more effective. Deformation enabled us to supply the H_2 gas molecules in a very low flow rate by using a shorter length of the capillary pipe even from a higher up stream pressure.

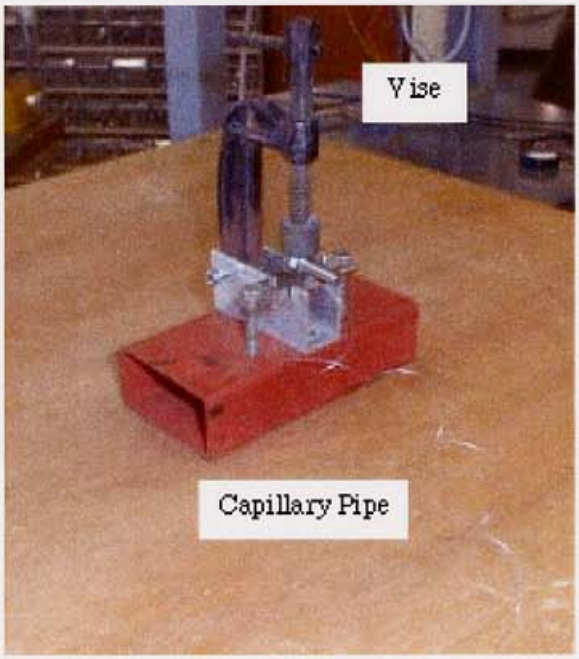

Figure 2.8: A simple gadget for making deformation of the capillary pipe.

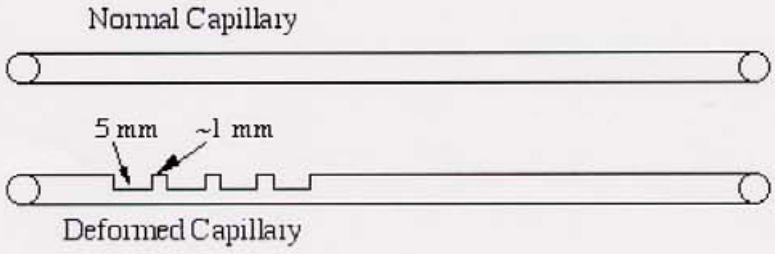

Figure 2.9: Structure of the deformation made by the gadget.

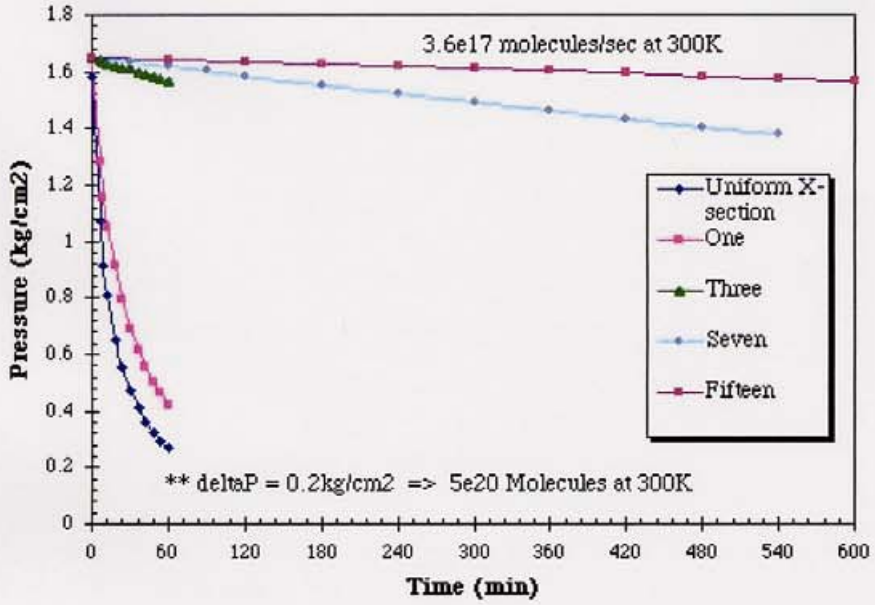

Figure 2.10: Flow rate of H_2 gas molecules through a 250 mm long capillary pipe as a function of number of deformation.

In our experimental setup, we used this deformed capillary pipe to control the admission of H_2 gas from the H_2 gas container into the vacuum chamber. Length of deformed capillary was 25 cm and number of deformation was 15. Figure 2.11 shows the gas flow control system. H_2 gas container was kept in a thermally insulated box in order to maintain the same temperature for sufficiently long time. Valve V4 was kept always open. By opening and closing the valve V5, an amount of H_2 molecules was admitted into the vacuum chamber. Number of H_2 molecules admitted into the vacuum chamber was determined by the ideal gas equation:

$$N = \frac{\Delta PV}{k_B T} \tag{2.1}$$

Where, V = 101.28 cc is the volume of the H_2 gas container, T is temperature in Kelvin of the H_2 gas container, k_B is the Boltzmann constant and ΔP is the pressure difference between before and after admission of gas into the vacuum chamber. Pressure of the H_2 gas container was measured with a digital manometer.

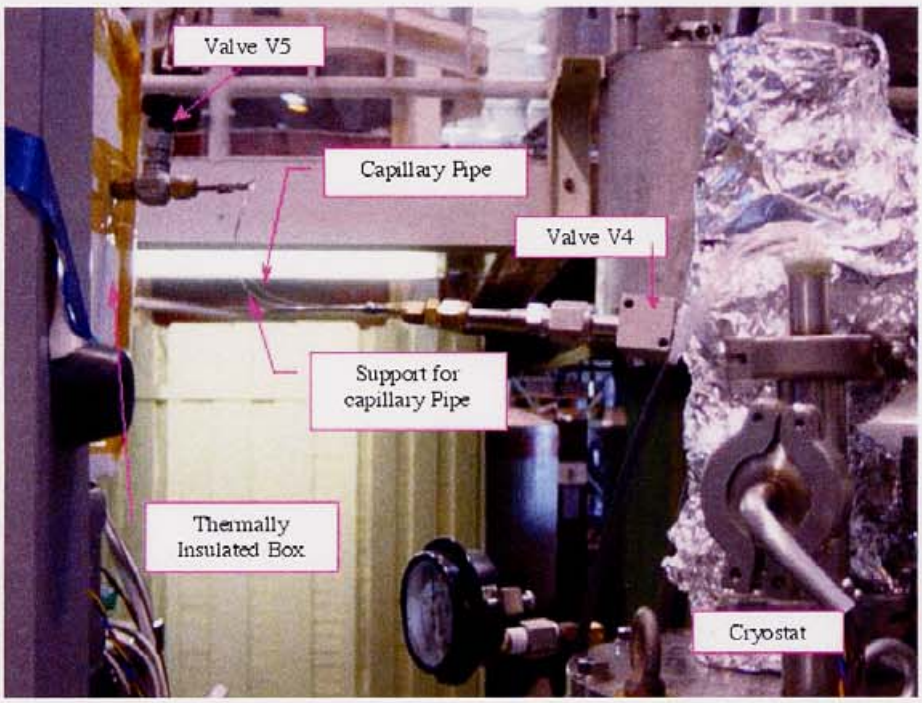

Figure 2.11: Gas flow control system. Sample gas container was kept inside a thermally insulated box.

2.2 Measurement System

For the measurement of total vacuum, Bayard-Alpert type ionization gauge was used at the top of vacuum chamber. A quadruple mass spectrometer (QMS) was used to measure the partial pressure of residual gas molecules. Relative position of the ionization gauge and QMS is shown in the Figure 2.1.

For the measurement of temperature, gold-iron chromel thermocouple is used. Temperature of the liquid helium inside the cryostat was used as the reference temperature. When the liquid helium was boiled off, liquid nitrogen was used as the reference temperature. Also copper-constantan thermocouple was used for the measurement of temperature above 0^0C.

A program in LabView was written to record the thermocouple voltages, total vacuum pressure and liquid helium level in the cryostat at an interval (Least interval is 1 sec). Our experiment took a very long time, even sometimes more than 24 hours. This resulted a huge amount of raw data of temperature as voltage. Another program was written in Mathmatica to convert these thermocouple voltages into temperatures.

2.3 Adsorption Experiment

2.3.1 Experimental procedure

Vacuum of the vacuum chamber was prepared by baking at 150^0C for 24 hours. Not only the vacuum chamber, but also the connecting vacuum pipe and bellow was also baked at 150^0C. Usually a vacuum of the order of 10^{-6} Pa was achieved at room temperature ($\sim$ 27^0C). After admission of liquid helium into cryostat, pumping of the pumping unit was stopped by closing the metal angle valve V3 shown in Figure 2.1. In our experiment we tried our best to make the temperature around the connecting flange area higher than the temperature of liquid helium. For this purpose, as mentioned in § 2.1.2, an annular vacuum space around the connecting vacuum pipe was made and also, the upper heater was wound at the lower part of the connecting vacuum pipe. Moreover, as shown in Figure 2.12, the connecting flanges and the lower part of the connecting vacuum pipe were covered by the Styrofoam in order to avoid direct contact with the liquid helium. In the H_2 adsorption experiment, we thus enabled to maintain the temperature at the lower end (Sensor AuFe5, Figure 2.1) of the connecting vacuum pipe higher (roughly 20K) than the temperature (4.2K) of vacuum chamber.

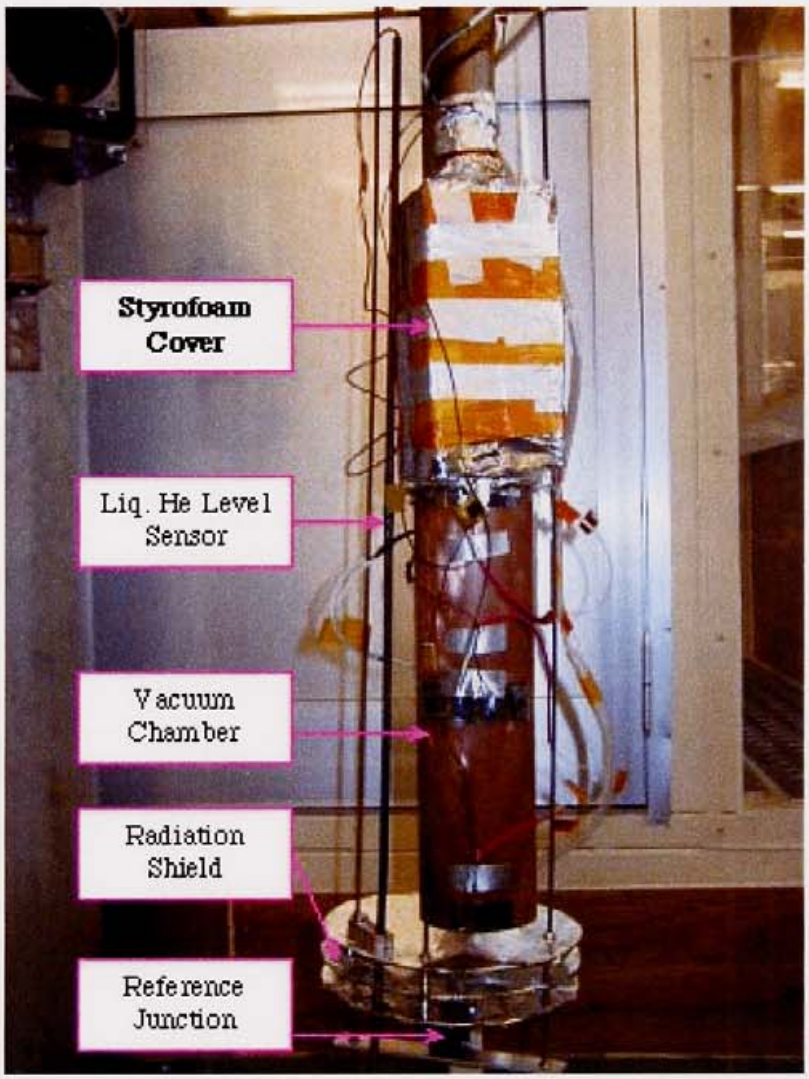

Figure 2.12: Styrofoam cover around the ICF flanges and lower part of the connecting vacuum pipe.

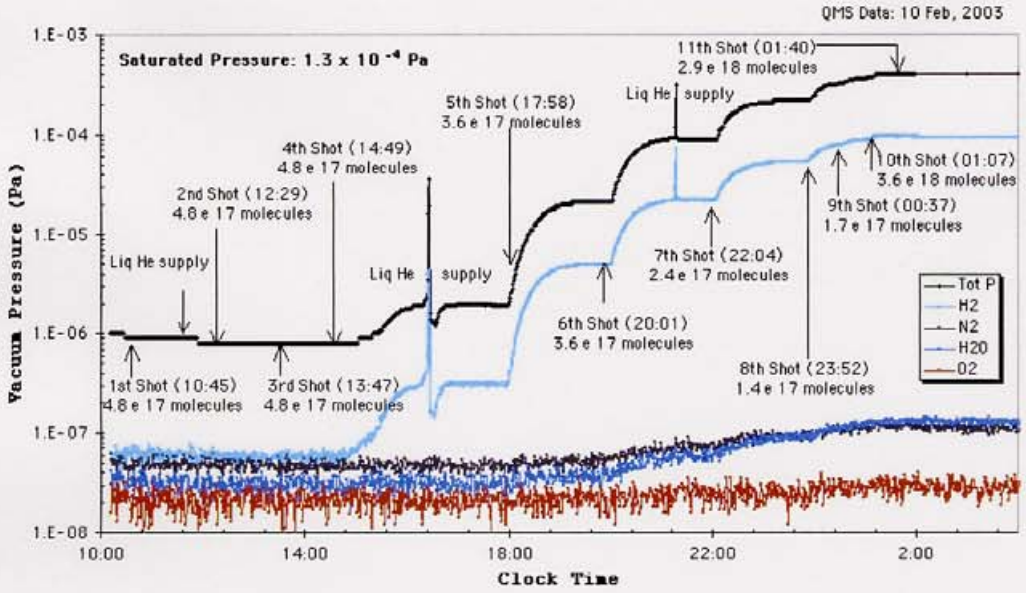

Figure 2.13: Adsorption of H_2 gas molecules in real time.

After achieving an equilibrium vacuum pressure at liquid helium temperature, an amount of H_2 gas molecules was admitted into the vacuum chamber by opening and closing the valve V5 (Figure 2.11). Valve V4 was kept open since the start of pumping of the vacuum chamber. Pressure and temperature of the H_2 gas container were recorded at the time of opening and closing the valve V5. We called the admission of H_2 molecules by opening and closing the valve V5 as a *shot*. Number of H_2 gas molecules admitted in a shot was calculated using Eq. (2.1). After each shot, we waited for the equilibrium pressure. Then another shot was admitted. In this way, H_2 gas molecules were admitted until the saturated pressure reached. At saturation, vacuum pressure remains constant although more and more H_2 gas molecules are admitted into the vacuum chamber.

Figure 2.13 shows how we carried out the experiment of H_2 desorption. After cool down the vacuum chamber at 4.2K, we usually waited for an hour to have an equilibrium pressure and then admitted the 1^{st} shot. An amount of 4.8 x 10^{17} H_2 molecules were admitted at the 1^{st} shot but no increase of either total pressure or the partial pressure of H_2 was observed in 45 minutes. Same amount of H_2 molecules were admitted at the 2^{nd} and 3^{rd} shot but no increase of vacuum pressure was observed. Soon after the 4^{th} shot, vacuum pressure started to increase and reached an equilibrium value in more than three hours. After achieving the equilibrium pressure, 5^{th} shot was admitted. In between the 4^{th} and 5^{th} shot, there was a sharp peak due to pouring the liquid helium into the cryostat. In this way, we continued the admission of H_2 molecules and reached the situation, where more and more H_2 molecules, for example, about 10 times H_2 molecules at 10^{th} and 11^{th}

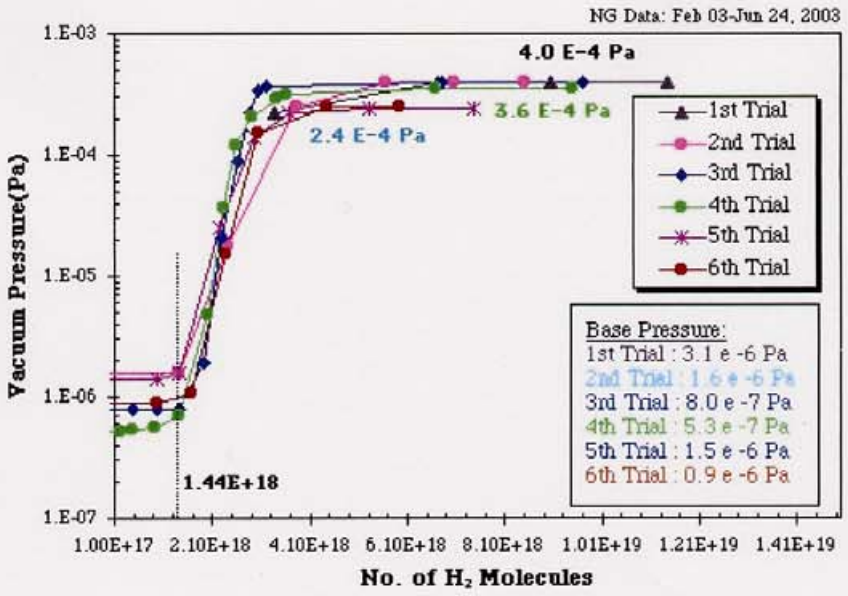

Figure 2.14: Vacuum pressure as a function of adsorbed H_2 molecules at 4.2K.

shots, were admitted without observation of increase of vacuum pressure. This indicated that vacuum chamber surface became saturated with the H_2 molecules. In the experiment shown in Figure 2.13, a saturated pressure of 3.8 x 10^{-4} Pa was recorded in the ionization gauge.

2.3.2 Results

From our experiment of H_2 adsorption, we learnt the equilibrium pressure as a function of number of H_2 molecules adsorbed on the copper surface at 4.2K. Figure 2.14 shows the equilibrium pressure as a function of H_2 molecules admitted into the vacuum chamber. There was no change or little change in vacuum pressure up to the adsorption of 1.4 x10^{18} H_2 molecules. For H_2 molecules more than this, vacuum pressure gradually increased to the saturated level. This revealed that adsorption of H_2 molecules up to 1.4 x 10^{18} was different from the adsorption of later molecules. What was the difference? This may be answered as follows. All H_2 molecules up to 1.4 x 10^{18} adsorbed on the vacuum chamber surface due to adhesive force between copper and H_2 molecules. The available surface was completely covered by these molecules. There was no room for any other H_2 molecules to be adsorbed directly with the copper surface. So, all other molecules adsorbed on the 1^{st} layer first, then on the 2^{nd} layer and so on. These molecules were loosely bound with the neighbor ones by the cohesive force. So, after formation of 1^{st} layer, equilibrium pressure

gradually increased with the adsorption of additional H_2 molecules and finally achieved a saturated state.

Our experiment showed that number of H_2 molecules required to form the monolayer was 1.4 x 10^{18} molecules. This value was very close to the calculated value 1.2 x 10^{18} (Table 2.1). This yielded that the surface roughness factor was almost one. Reason of this unit roughness was not clear. But it may be worthy to consider that our vacuum chamber was made from that OFHC copper cylindrical pipe, which was made from the cylindrical rod by extrusion. Moreover, vacuum of our vacuum chamber was not so high.

Our experiment also revealed that only a few layers of H_2 molecules were enough to attain the saturated vacuum pressure. Saturated pressure of H_2 on copper surface at liquid helium temperature was of the order of 10^{-4} Pa. This value agrees with the earlier result[21].

2.4 Desorption Experiment

2.4.1 Experimental Procedure

After the adsorption experiment, we started the desorption experiment. At first liquid helium level in the cryostat was checked and maintained up to the top of vacuum chamber as the initial condition of the desorption experiment. Then, by opening the metal angle valve V3 (Figure 2.1), pumping of the pumping unit was brought in action. Otherwise, due to warm up, pressure of the vacuum chamber increased very fast beyond the measurable condition of the ionization gauge and the quadruple mass spectrometer. Due to pumping, vacuum pressure decreased from the saturated pressure 10^{-4} Pa to a lower pressure as shown in Figure 2.15.

It is very important to separate the desorption occurred at the vacuum chamber from the desorption of the same molecules occurred outside the vacuum chamber. For this purpose, temperature around the connecting flanges and the lower part of the connecting vacuum pipe was maintained higher compared to the temperature of the vacuum chamber as shown in the Figure 2.15. This way of maintaining temperature also ensured us that the molecules, which were desorbed from the vacuum chamber, did not get cryo-trapped outside the vacuum chamber.

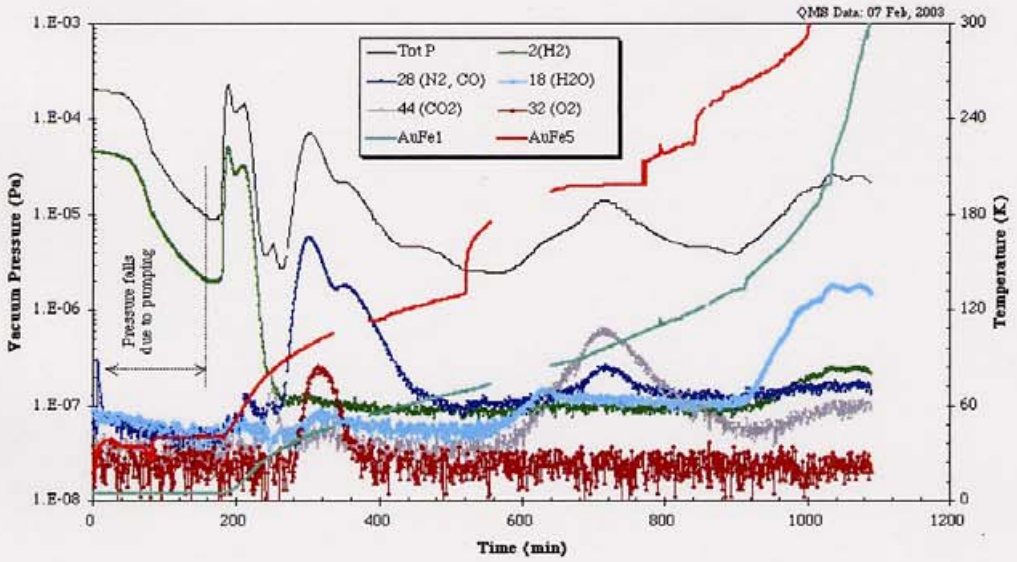

Figure 2.15: Desorption time curve. Positions of thermo-sensors AuFe1 and AuFe5 are shown in Figs. 2.1 & 2.3.

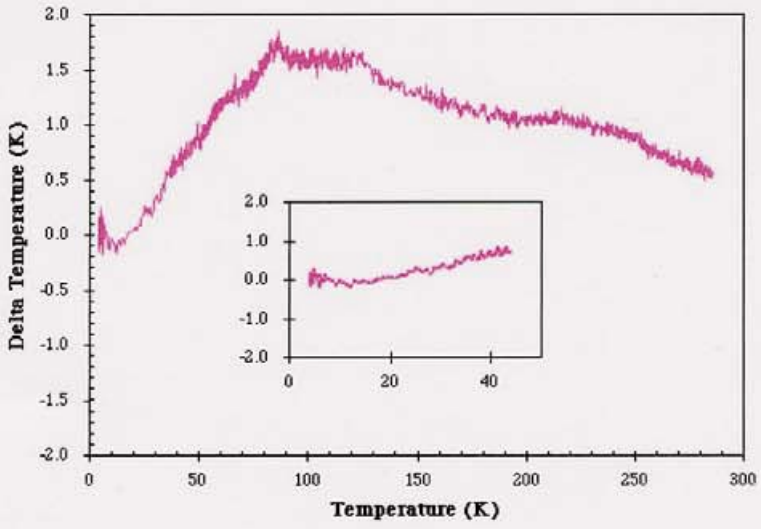

Figure 2.16: Temperature difference between the two ends (thermo-sensors AuFe1 and AuFe3) of vacuum chamber as a function of temperature of the lower end.

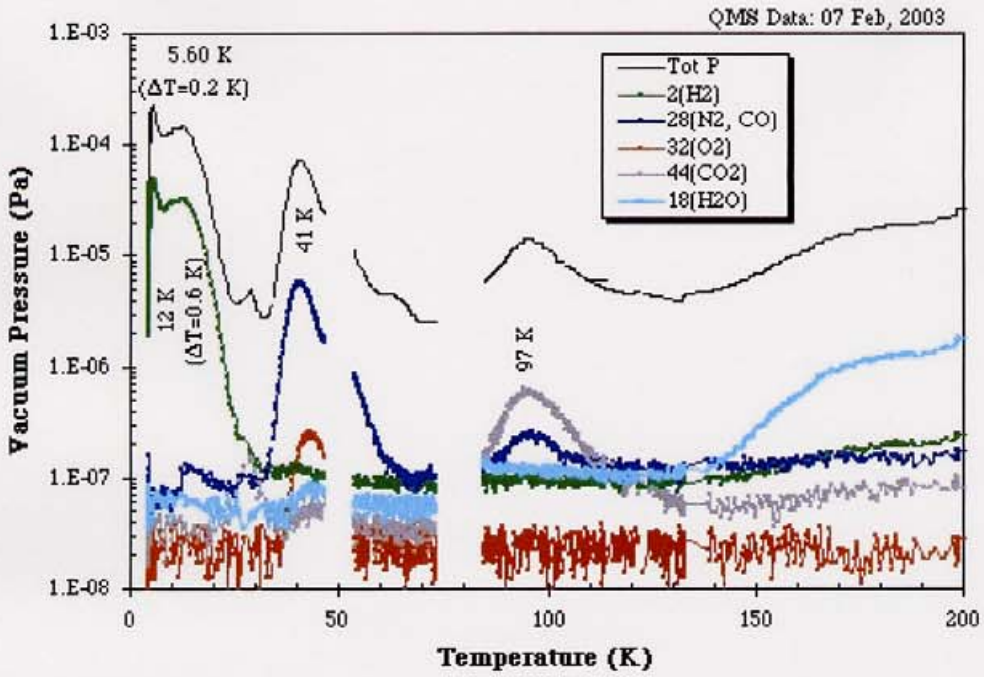

Figure 2.17: Desorption of adsorbed molecules as a function of temperature from the H_2 saturated surface.

During the warm up of the vacuum chamber, temperature distribution along the length of the vacuum chamber was tried to keep very low as shown in Figure 2.16. Warming was done by the simultaneous use of both the upper and bottom heaters. Control of increase of temperature was very difficult, particularly after the boil off of liquid helium. So, it was hard to follow the same time profile of warming in all desorption experiments.

2.4.2 Results

Figure 2.17 shows the desorption of H_2, N_2, CO, CO_2 and H_2O adsorbed on the copper surface. We prepared the copper surface saturated by H_2 at 4.2K. Desorption of H_2 appeared as a sharp peak around 5.6K followed by another broad peak around 14K. Why did desorption of H_2 appear as two peaks? We thought that desorption from layers other than the monolayer made the first sharp peak and second broad peak was due to desorption from the monolayer.

This explanation of the two peaks prompted us to carry on experiment to study the desorption from the 1st monolayer. From our adsorption experiment, we learnt the number of H_2 molecules required to form the monolayer (§ 2.3.2). By admitting a less amount

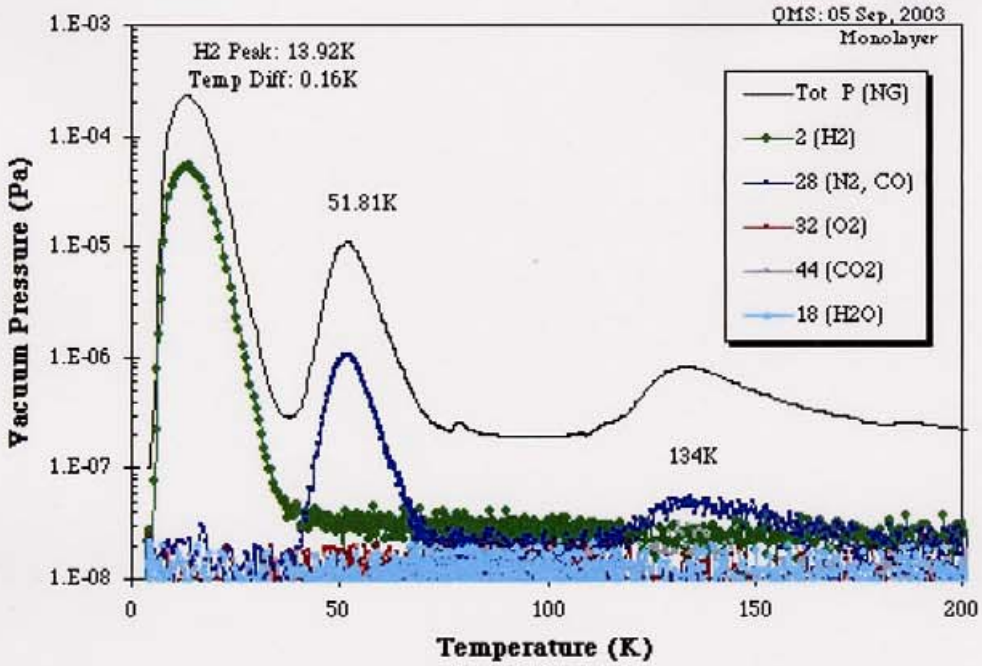

Figure 2.18: Desorption from H_2 monolayer surface as a function of temperature.

of H_2 molecules than the amount required to form the monolayer, we built up a partial monolayer of H_2 at liquid helium temperature. Then the vacuum chamber was warmed up as mentioned in § 2.4.1. Figure 2.18 shows the desorption from the H_2 monolayer surface. In this case, desorption of H_2 has only one broad peak around 14K, there is no sharp peak around 5.6K, as we observed during the desorption from H_2 saturated surface. This confirms our explanation. Figure 2.19 shows that the broad peak of H_2 desorption of from multilayer surface can be explained by the H_2 desorption from the monolayer surface of H_2. It should be noted that peak height depended dominantly on the rate of warming and the same time profile of warming could not be maintained in all the trials.

During the desorption of H_2 molecules, temperature difference between the top and bottom of the vacuum chamber was of the order of 0.1K whereas peak width at half maximum of the H_2 desorption peak was about 20K. So, width of desorption peak in our experiment was not due to the temperature distribution along the length of the vacuum chamber. The large peak width may be explained as that all the molecules become agitated but by chance, a molecule can acquire the sufficient energy to come out from the surface.

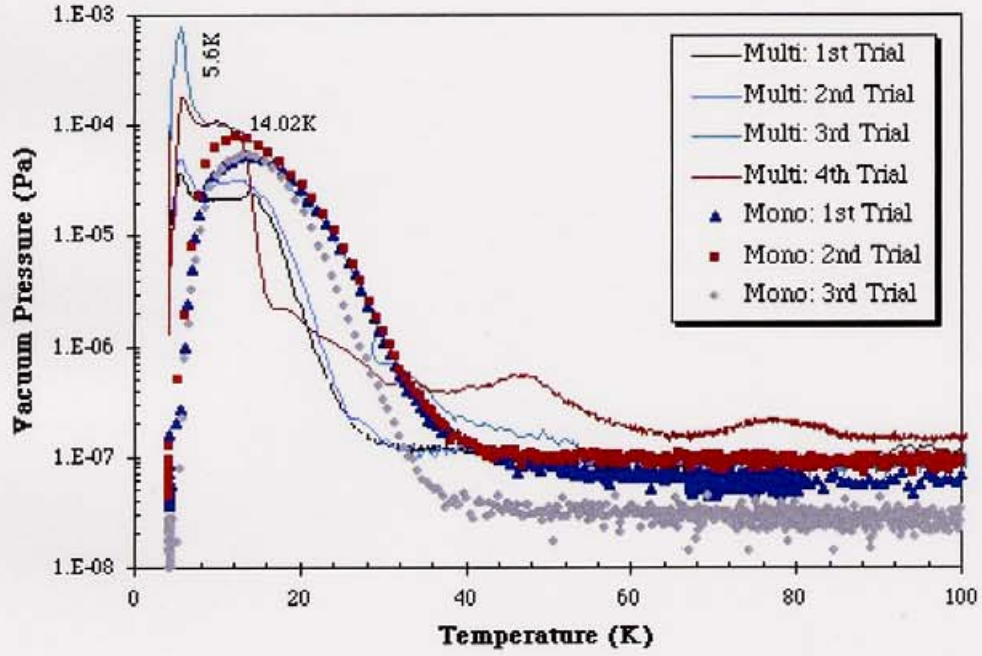

Figure 2.19: Desorption of H_2 from monolayer and multilayer of adsorbed H_2 as a function of temperature.

Chapter 3

Multipacting Experiment

In order to study the multipacting, we developed a dedicated experimental setup. Our prime interest is in the origin of multipacting. So, rather than using an existing cavity built for accelerators such as KEKB Crab cavity, we built a multipacting prone cavity. Then we studied the multipacting regarding the adsorption of two dominant residual gas molecules H_2 and CO.

3.1 Design of RF Cavity

From the experience of cavity experiment, it was found that multipacting occurs severely at the coaxial part of the cavity. This was also explicitly revealed in the research and development of KEKB Crab cavity. A coaxial cavity, therefore, seems to be very prone to multipacting. That's why we decided to build up a coaxial type cavity.

During the very first stage of the cavity design, we considered the different options of rf power source. Magnetron available from the used domestic microwave oven seemed very promising because of its high rf power (500W or more) at a low price. But the magnetron designed for the domestic microwave oven has a fixed frequency 2.45 GHz. So, some tuning mechanism should be adopted into the cavity structure. This makes the cavity structure complex. We preferred the simple structure as much as possible for the easier understanding of the experimental events. So, instead of using magnetron, we opted for the use of a broadband amplifier such as Traveling Wave Tube (TWT) amplifier.

Resonant frequency was chosen as 1.5 GHz so that the rf system developed for the R&D of 1/3 Crab cavity could be used in our experiment.

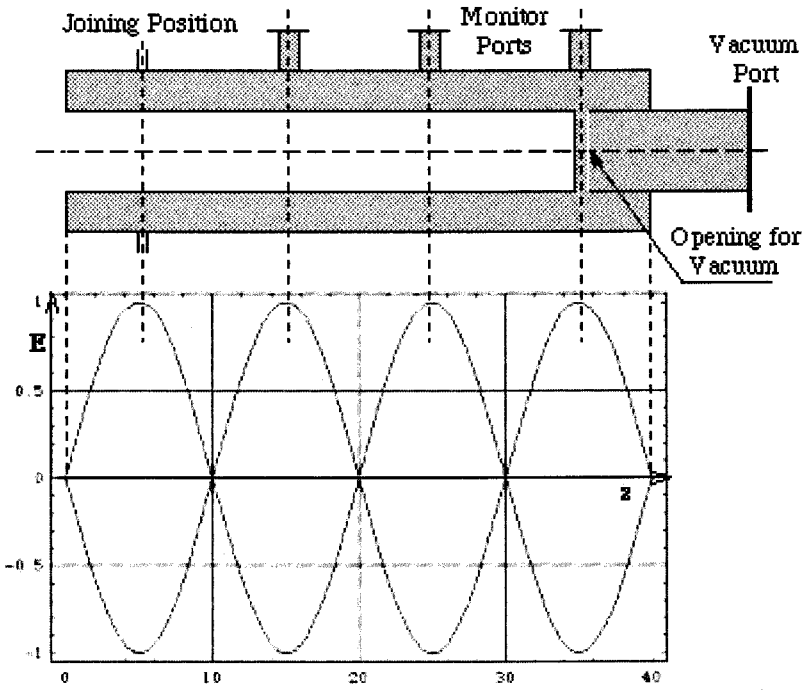

Figure 3.1: Conceptual design of the coaxial cavity.

Figure 3.1 shows the conceptual design of the 1.5 GHz coaxial cavity. Mode of excitation was so chosen that different cutting parts, for example, vacuum opening at inner conductor, were at the places where rf surface current was zero. This mode selection allowed us to build up a coaxial cavity of rather high unloaded Q_0. Figure 3.2 shows the detailed design of the coaxial cavity. Most important feature of our design is that inner conductor can be taken off from the outer conductor. So, our design provided different options to study the multipacting. For example, we can easily change the surface condition at the probable multipacting site.

3.2 Fabrication of RF Cavity

Outer conductor was made from oxygen free high conductivity (OFHC) copper pipe. This copper pipe was made from cylindrical bar by extrusion. For inner conductor and probe port, copper pipe was used. End plates were made from copper sheet. Flanges were made of SUS. All parts were joined by vacuum silver brazing. Indium seal was used to join the inner conductor with the outer conductor. Figure 3.3 shows the coaxial cavity after fabrication.

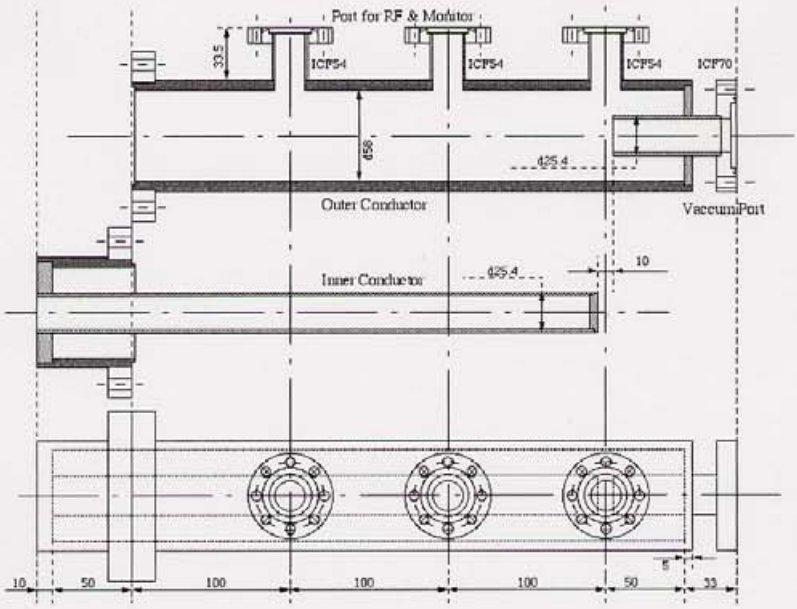

Figure 3.2: Real design of the coaxial cavity.

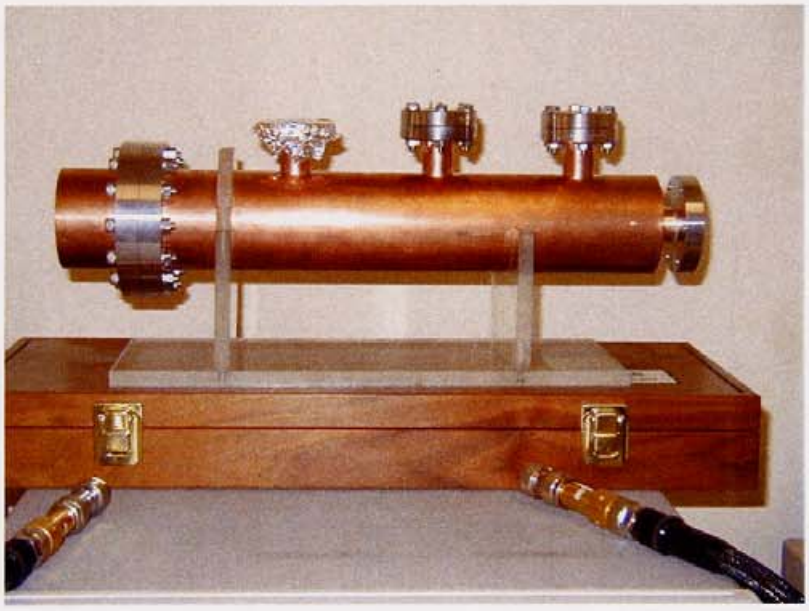

Figure 3.3: Our designed coaxial cavity.

3.3 RF Field and Quality of the Coaxial Cavity

Due to cylindrical symmetry, there is only radial component of electric field (E_r) and corresponding azimuthal magnetic field (H_ϕ). On the assumption of perfect reflection at the both ends of the cavity, electromagnetic fields can be expressed as follows [1]:

$$E_r = Z_0 \frac{I_0}{\pi r} \cos(\beta z) \exp(j\omega t) \tag{3.1}$$

$$H_\phi = j \frac{I_0}{\pi r} \sin(\beta z) \exp(j\omega t) \tag{3.2}$$

Here, Z_0 is the intrinsic impedance of the medium inside the cavity. For our coaxial cavity, $Z_0 = 377\Omega$. I_0, peak rf surface current, can be expressed in terms of resonant frequency (f), input rf power (P), cavity length (L) and unloaded quality (Q_0) as follows:

$$I_0 = \sqrt{\frac{PQ_0}{\mu_0 f L \ln(\frac{b}{a})}} \tag{3.3}$$

At the both ends of the cavity, electric field (E_r) must be zero. This condition defines the allowed resonant modes:

$$\lambda_N = \frac{2L}{N} \; ; \qquad N = 1, 2, 3, \ldots \tag{3.4}$$

We chose the designed mode $N = 4$. This required that resonant wavelength (λ_0) is half of the length of the cavity. Unloaded quality (Q_0) for the design mode of excitation can be expressed by the following equation:

$$Q_0 = \frac{1}{\delta_s} \frac{1}{\frac{2}{L} + \frac{1}{2b} \frac{1+\frac{b}{a}}{\ln(\frac{b}{a})}} \tag{3.5}$$

Here, δ_s is the skin depth. At our design frequency 1.5 GHz, skin depth of Cu is 1.7 μm at 20^0C. Parameters a and b are the radius of inner and outer conductor, respectively. For our cavity, L = 40 cm, a = 1.27 cm and b = 2.9 cm. Table 3.1 shows the calculated value of Q_0 and the corresponding electric field (E_{sp}) at input rf power 200W at 20^0C and liquid nitrogen temperature (-196^{0}C).

[1] Detailed derivation is given in Appendix-A

Table 3.1: Calculated Q_0 and E_{sp} at rf input power 200W

Temperature (K)	Q_0	E_{sp}(kV/m)	
		At inner conductor	At outer conductor
293	7964	478	209
77.3	2.34×10^4	819	359

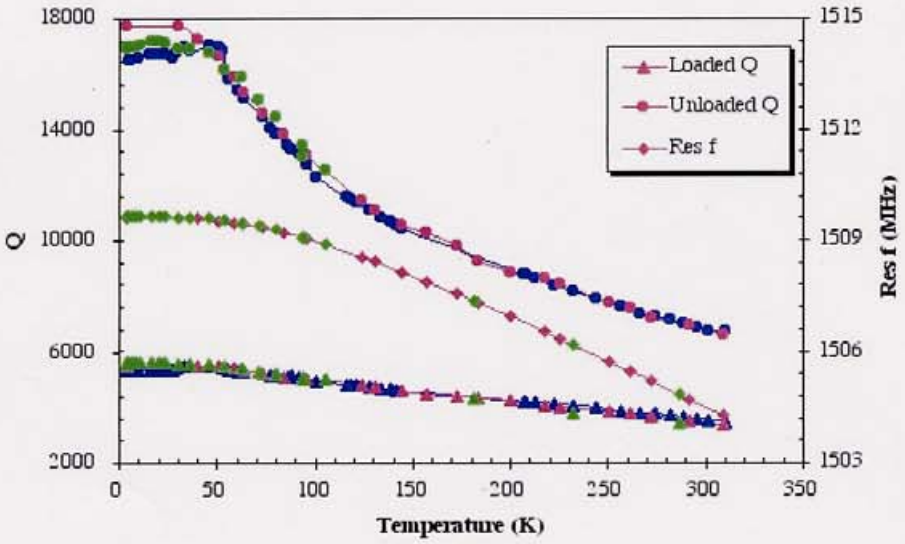

Figure 3.4: Measured value of quality Q_L, Q_0 (=Q_L x β_{in}) and resonant frequency f_0 as a function of temperature.

We measured the Q_0 as a function of temperature with the different probes set at the positions mentioned in Table 3.3. Figure 3.4 shows the measured value of loaded quality Q_L, unloaded quality Q_0 and resonant frequency f_0 as a function of cavity temperature. Unloaded quality Q_0 was determined by the product of Q_L and input coupling coefficient β_{in}. Measured value of Q_0 at 20^0C was around 7000, which was very close to the calculated value mentioned in Table 3.1. This agreement showed that although the inner conductor was cut away by 10 mm for the vacuum opening, we enabled to achieve the Q_0 close to the calculated value and this was due to our selection of the excitation mode. This agreement also indicated that joints between different parts of our cavity were very well at room temperature. This might be not true at liquid helium temperature. So, the measured Q_0 of the cavity at liquid helium temperature was rather low, around 17000.

Table 3.2: Measured Q_0 and corresponding E_{sp} at rf input power 200W

Temperature (K)	Q_0	E_{sp}**(kV/m)**	
		At inner conductor	**At outer conductor**
293	7000	448	196
4.2	1.7×10^4	692	306

In the case of input coupler of KEKB superconducting accelerating cavity, peak electric fields at inner and outer conductor are 0.25 and 0.11 MV/m, respectively, in traveling wave mode at rf power 300 kW. The field level of the input coupler is low compared to that of our coaxial cavity. So, our experiment can reproduce the multipacting observed in the input coupler of KEKB superconducting accelerating cavity.

3.4 Probe Design

Unfortunately, our cryostat was too slim to have room for a probe of adjustable length. Moreover, we had limitation of input rf power. So, it was necessary to design the input probe of unit coupling (β_{in} =1).

In order to find out the length of probe required for unit coupling, we, at first, designed a probe of adjustable length for the use at atmospheric pressure. Figure 3.5 shows the design of this probe. This designed probe was used in the measurement of coupling factor β_{in} as a function of probe length . Figure 3.6 shows the photograph of the measurement. In the measurement, probe length was measured from the inner surface of the outer conductor. Our definition was that if the tip of probe was inserted deep more than the inner

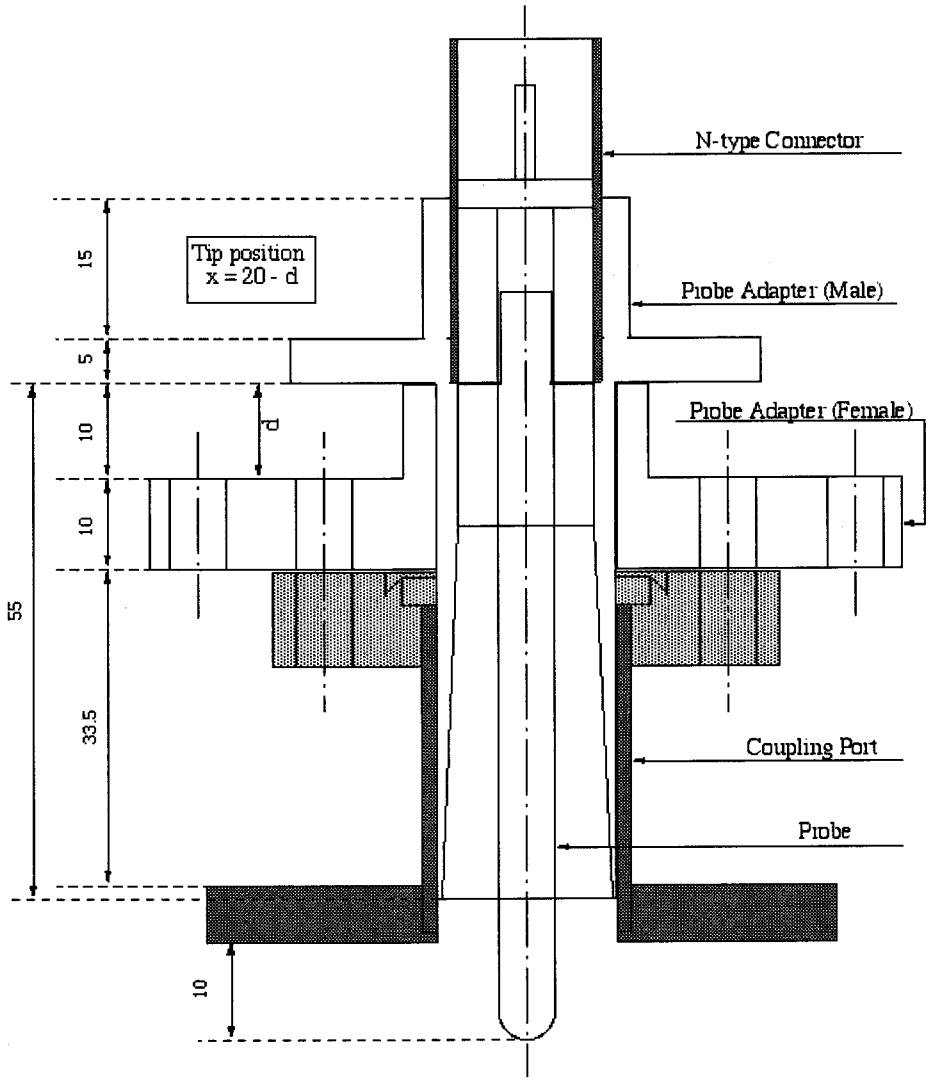

Figure 3.5: Design of adjustable length probe.

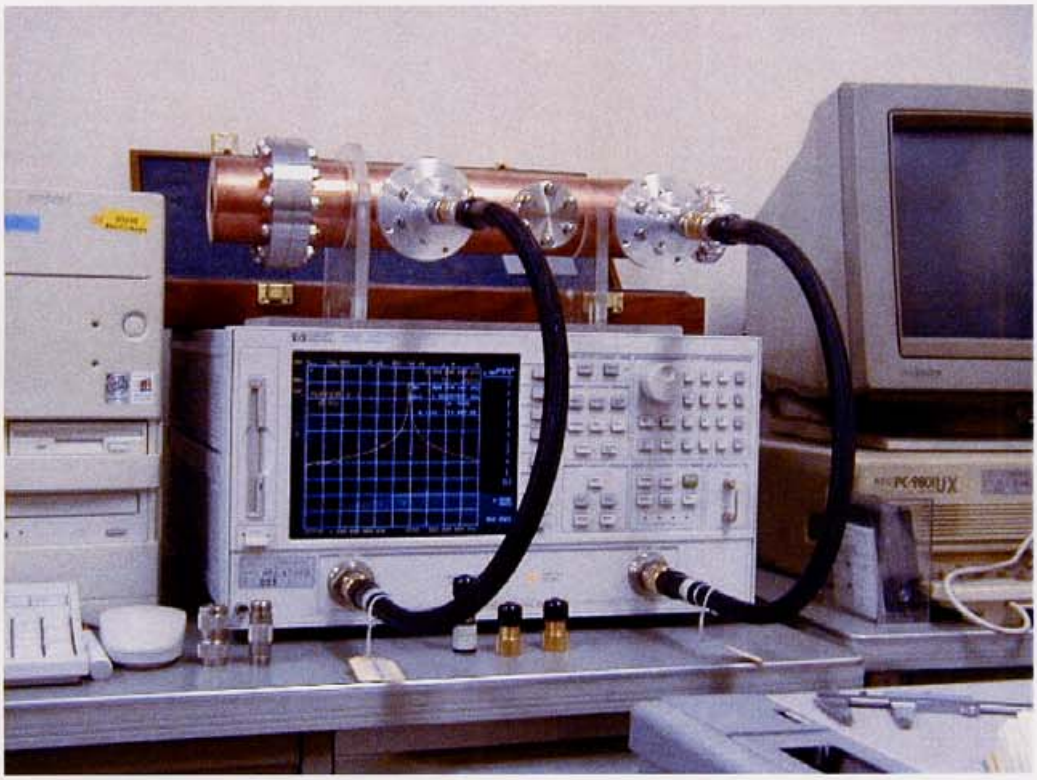

Figure 3.6: Measurement with Network Analyzer for determination of the probe length required for unit coupling.

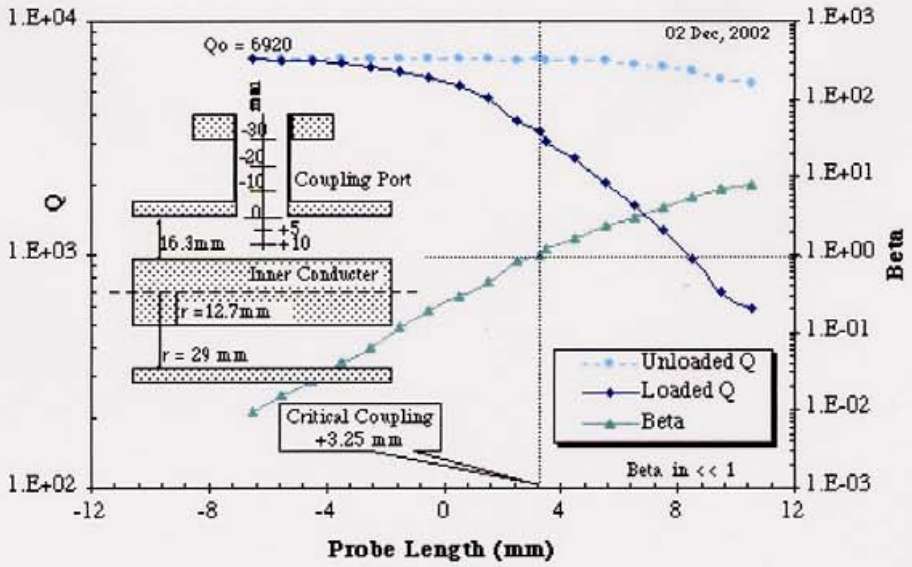

Figure 3.7: Quality Q_L, Q_0 and β_{in} as a function of the probe length. Inset figure shows the definition of length measurement.

surface of the outer conductor, then the length was taken as positive, otherwise negative. Figure 3.7 shows the quality factor Q_L, Q_0 and β_{in} as a function of the probe length. For unit coupling, tip of the probe should be at a distance +3.25 mm from the inner surface of the outer conductor.

Knowing the required length of probe, we designed the probe for experiments with ultra high vacuum. Figure 3.8 shows the probes made for the multipacting experiments. Right most one was designed for unit coupling and, hence, was used as the input probe. Other two probes had coupling factor less than unity and were used as monitor and transmission probes. After mounting the probes into the cavity, coupling factors were measured using the Network Analyzer. Table 3.3 shows the measured values of coupling factors of the different probes.

Table 3.3: Coupling factors of different probes

Probe	**Tip Position mm**	β
Input Probe	+3.275	1.02
Transmission Probe	-5.525	0.01
Monitor Probe	-9.225	0.0015

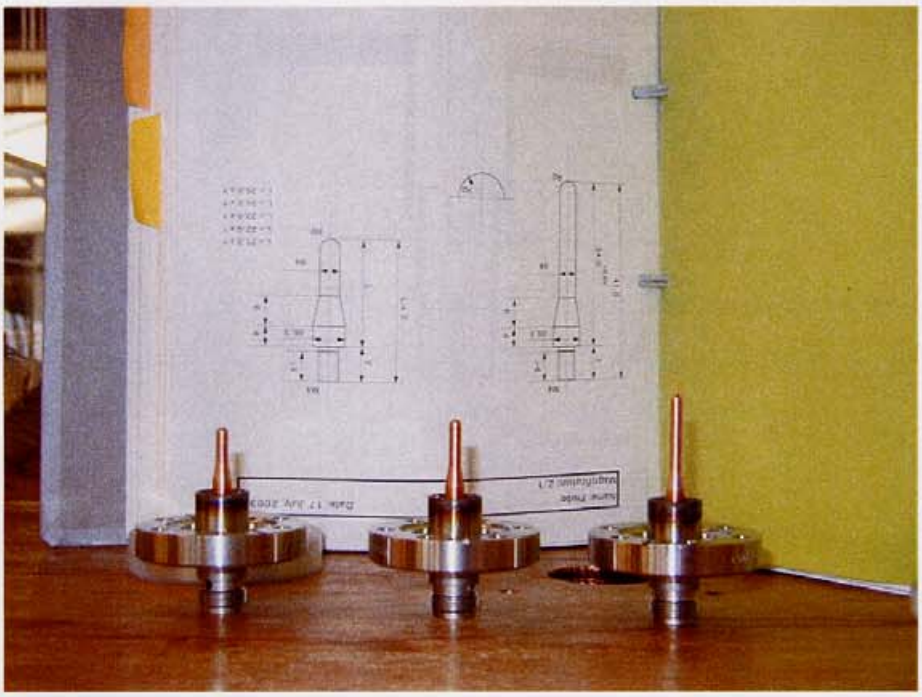

Figure 3.8: Designed probes for multipacting experiments.

3.5 Design of Cryostat Top Flange

Figure 3.9 shows the design of cryostat top flange. Concept of design was almost same as that described in § 2.1.2; only difference was the position of the connecting vacuum pipe. Probes made the coaxial cavity cylindrically asymmetric. In order to accommodate the cavity, we had to shift the connecting vacuum pipe radially outward. We also designed an adapter to mount the different vacuum gauges and pumps. Figure 3.10 shows our designed cryostat top flange and the adapter.

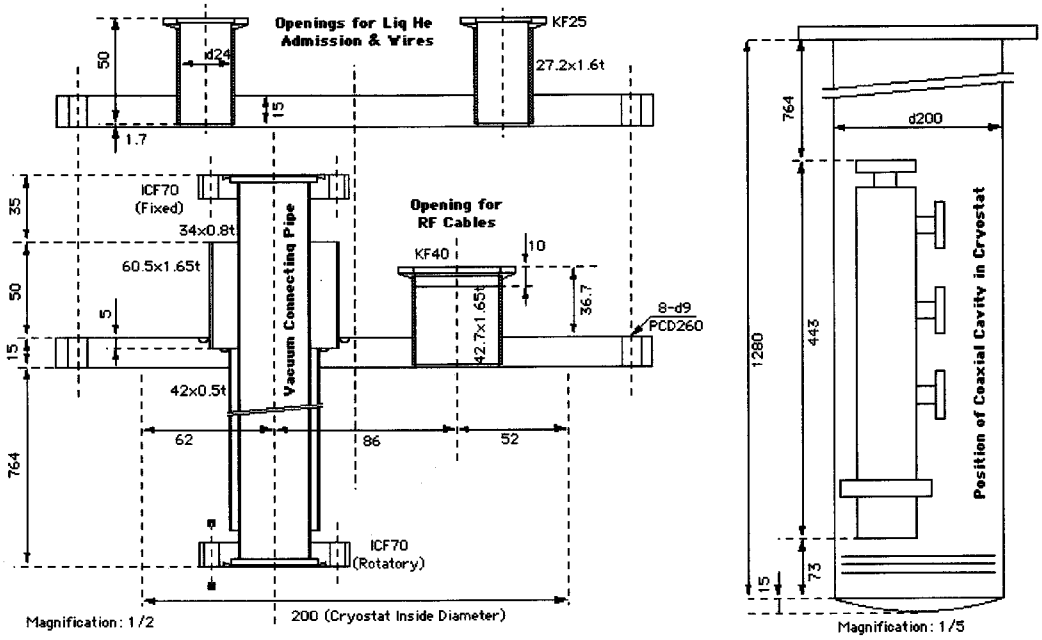

Figure 3.9: Design of cryostat top flange for set up the coaxial cavity into the cryostat.

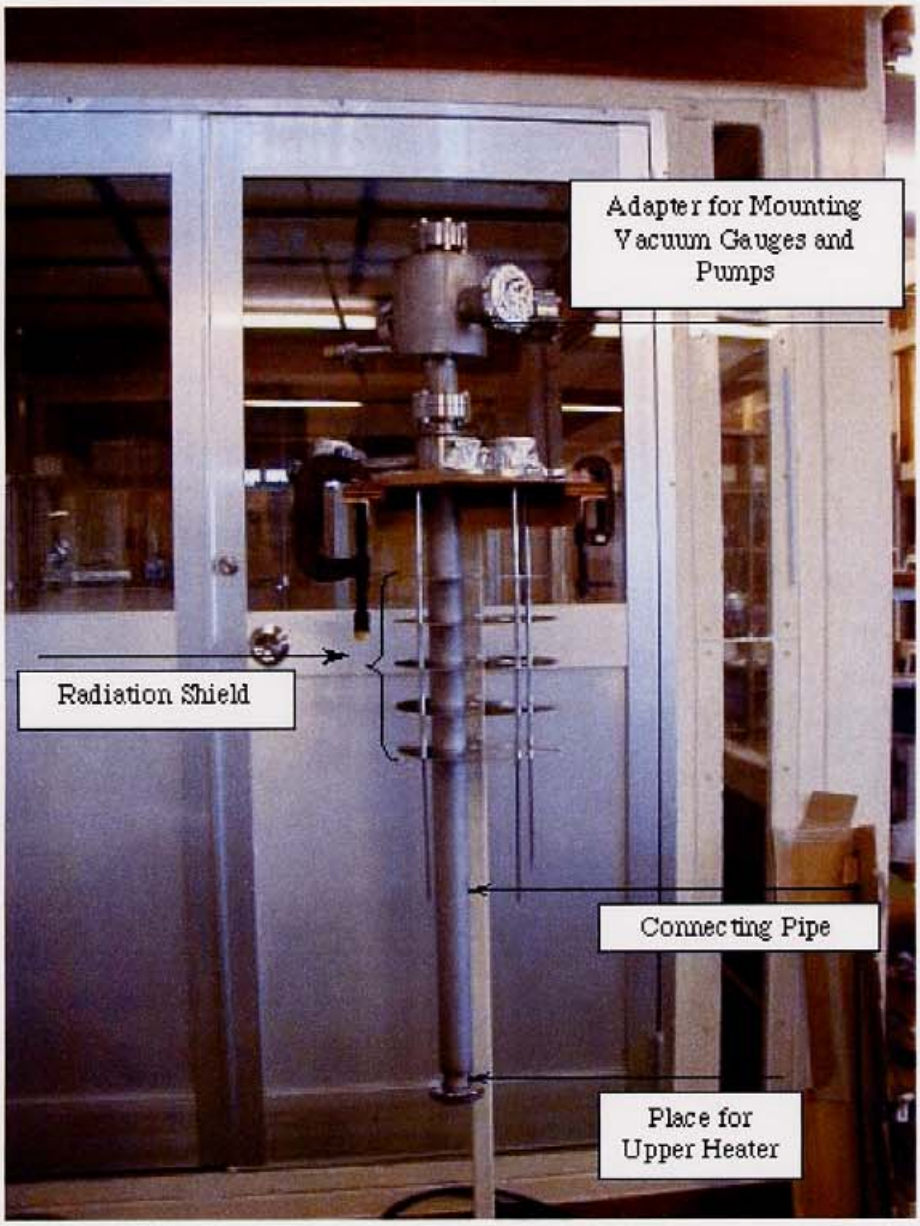

Figure 3.10: Our designed cryostat top flange and adapter for mounting different vacuum gauges and pumps.

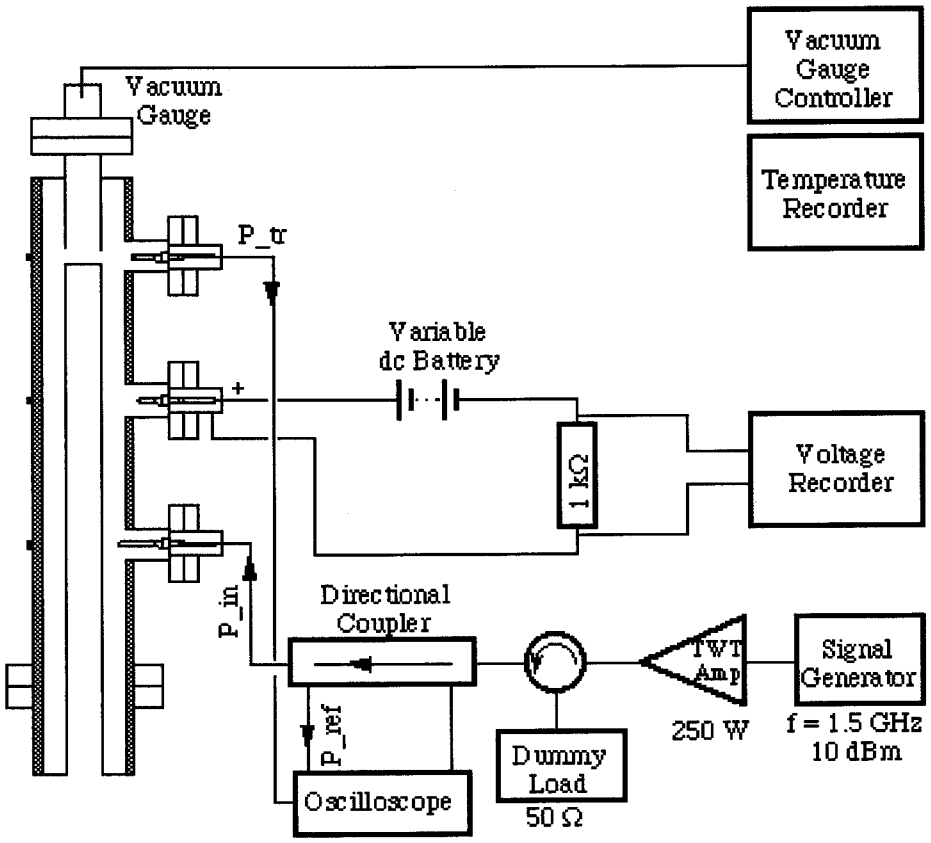

Figure 3.11: Schematic view of setup of multipacting experiment.

3.6 Experimental Setup

Figure 3.11 shows the experimental set up schematically. A combination of a signal generator and a traveling wave tube (TWT) amplifier was used as the source of rf power. By using this rf power source, we enabled to have the input rf power up to 200W. Reflected and transmitted signal coming out from the cavity were used to study the multipacting. Also, current due to multipacting electrons was measured to study the multipacting. Multipacting electrons were collected by using a very simple electric circuit as shown in Figure 3.11. And, Figure 3.12 shows the current due to multipacting electrons as a function of dc bias voltage. We have found that a +30V was enough to collect the multipacting electrons in our setup. Due to impact of multipacting electrons on the cavity surface, desorption of the adsorbed gas molecules takes place and thus the vacuum pressure of the cavity increases. Figure 3.13 shows the desorption of different gas molecules during multipacting at room temperature. We also monitored this increase of vacuum pressure to study the multipacting at room temperature. At liquid helium temperature it was very hard to detect this desorption due to multipacting electrons because desorbed molecules again got adsorbed at the place where multipacting did not take place.

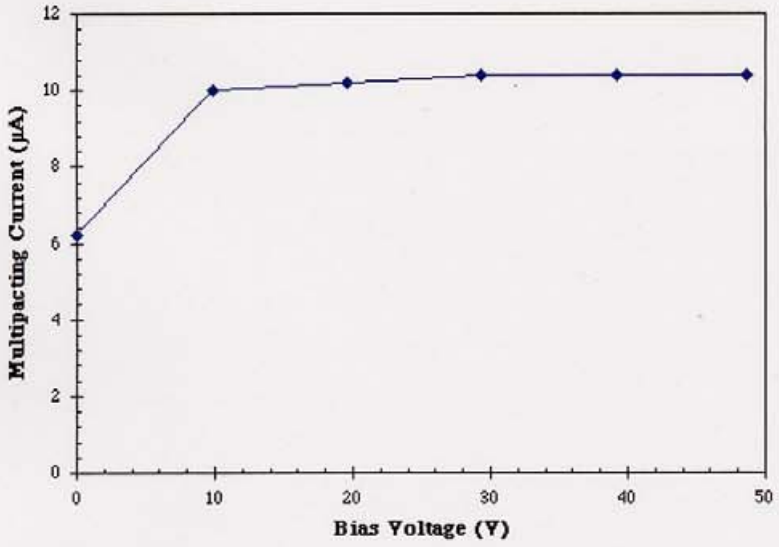

Figure 3.12: Current due to multipacting electrons as a function of bias voltage.

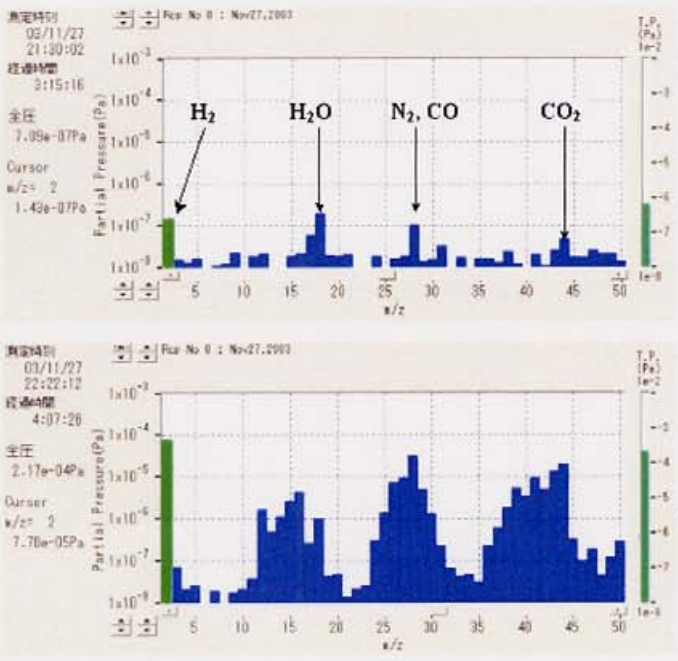

Figure 3.13: Desorption due to bombardment of multipacting electrons with cavity surface. Upper one shows the vacuum state just before start of rf excitation and lower one shows the vacuum state during multipacting.

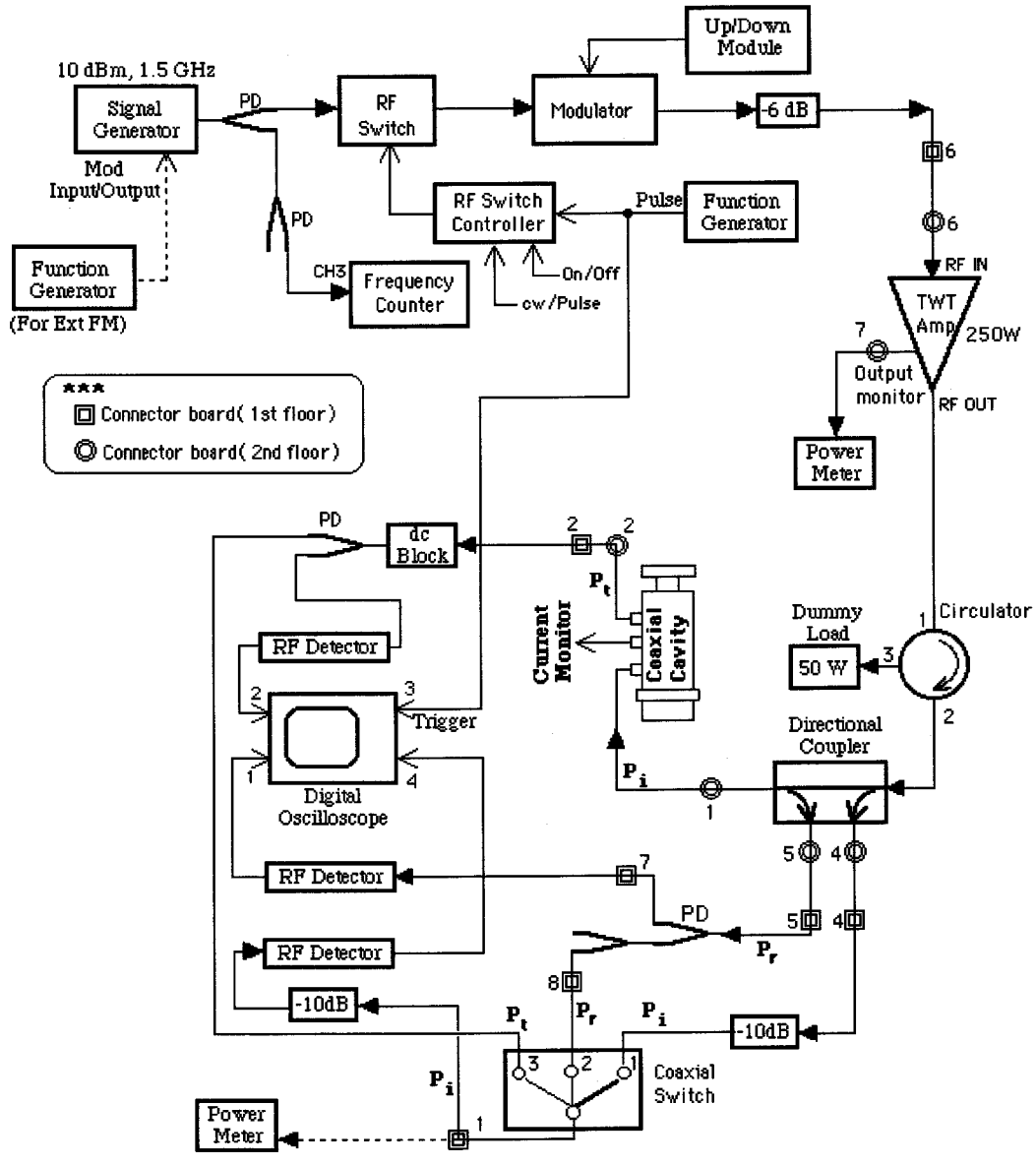

Figure 3.14: Schematic diagram of the rf system.

Figure 3.14 shows the schematic diagram of the rf system used in our experiment. This system was originally developed for the study of 1/3 superconducting Crab cavity. Since our coaxial cavity was a normal conducting cavity, the feed back loop for adjustment of the resonant frequency was not used in our setup. In the study of Crab cavity, power requirement was too low compared that of our experiment. So, the rf system could not handle such a high power in continuous mode. Instead of continuous power, we carried on our experiments by feeding the rf power in pulse mode. Frequency of pulse was 1 Hz and pulse width was 36 msec during which rf power was fed into the cavity.

3.7 Experiments

3.7.1 Procedures

Before the start of the experiment, resonant frequency was searched at low rf power (0.2W) in continuous mode. Then the mode of input rf power was switched into the pulse mode. rf power in pulse mode was continuously fed in to the cavity until there was no indication of multipacting. Initiation of multipacting was detected by observing the current due to multipacting electrons and reflected and transmitted signals in digital oscilloscope. During experiment at room temperature, we also monitored the vacuum pressure of the cavity to determine the onset of multipacting. As soon as multipacting started, increase of input rf power was halted. When multipacting seemed to be processed, again rf power was slowly increased until the next multipacting incident. In this way, experiment was carried on up to the available maximum power.

Although multipacting events were extremely fast (order of a few rf time periods), we found that a low response analog system was very convenient and efficient to study the gross feature. We used Pen Recorder[2] to simultaneously record the vacuum pressure, controlling voltage of input rf power and current due to multipacting electrons. As mentioned in § 3.6, the coaxial cavity was driven by rf power only for 36 msec in each second. On the contrary, the characteristic time constant (τ, defined by $Q_L = 2\pi f\tau$) of our cavity is of the order of microsecond. In our experiment, therefore, the coaxial cavity could store rf energy for less than 36 msec in each second. So, if there was an onset of multipacting incidents, it continued like initiated and ceased in each second until the multipacting became processed down. For this reason, multipacting current recorded in Pen Recorder chart appeared as the continuous series of spikes.

[2]LR4200E, Yokogawa, Japan.

3.7.2 Room Temperature Multipacting

At first, we studied the multipacting incidents at room temperature (~298K) by preparing the cavity vacuum of the order of 10^{-6} Pa at room temperature (~20^0C) without baking. Figure 3.15 – 3.18 shows the multipacting incidents at room temperature recorded in the Pen Recorder chart[3]. These multipacting incidents were observed during the very first rf excitation after exposing the cavity to the ambient air. To explain the multipacting qualitatively, we used some comparative terminologies such as hard, soft, strong and weak. *Strongness or* weakness was the measure of current due to multipacting electrons. For example, at input power of 182W, pen recorder recorded a large spike of multipacting current followed by two small spikes as shown in Figure 3.18. This large spike was categorized as strong multipacting in comparison to the smaller spikes categorized as weak multipacting. *Hardness or* softness was the measure of time required to process a multipacting incident. For example, multipacting at 60W shown in Figure 3.16, became processed by 12 minutes whereas multipacting at 129W shown in Figure 3.17, did not become processed within 140 minutes. Multipacting at 61W was categorized as a soft incident as compared to that at 129W categorized as hard incident.

During the very first rf excitation after preparation of vacuum from the expose to ambient air, first multipacting was observed at input power of around 15W (123 kV/m) [4]. As illustrated in Figure 3.15, this incident was so weak that it was very hard to detect the multipacting current by our simple measuring circuit. This incident was soft as well. A few incidents like this were observed for input power below 60W (246 kV/m). First strong multipacting was observed at input power of around 60W (Figure 3.16). It took the longest time, around 15 minutes, to become processed. After this incident, strong incidents were observed to occur with a small increase of input power. These multipacting took a few minutes to become processed. Multipacting incidents became very severe when the input power reached above 100W (317 kV/m). Below 100W, multipacting seemed to be processed sharply whereas above 100W, initial strong incident was followed by a continuous series of weak incidents; 70-80% processing time attributed these weak incidents. As the input power increased, strong incidents occurred irregularly against the background of continuous series of weak incidents as shown in Figures 3.17 & 3.18. Sometimes multipacting seemed to be processed down but if rf power was fed for long time, it suddenly started again. Our available input power (180W) was not enough to surmount this hard barrier.

[3]Due to setting of the Pen Recorder, origin of time scale of vacuum pressure was ahead that of input rf power, which was again ahead of time scale of multipacting current. Difference is 2.5 minutes. It is very difficult to understand this difference in the given images of Pen Recorder Chart. So, all images of Pen Recorder Chart have been illustrated with some labels to minimize the different in origin of time scales.

[4]From now on, peak electric field at inner conductor is mentioned in the parenthesis.

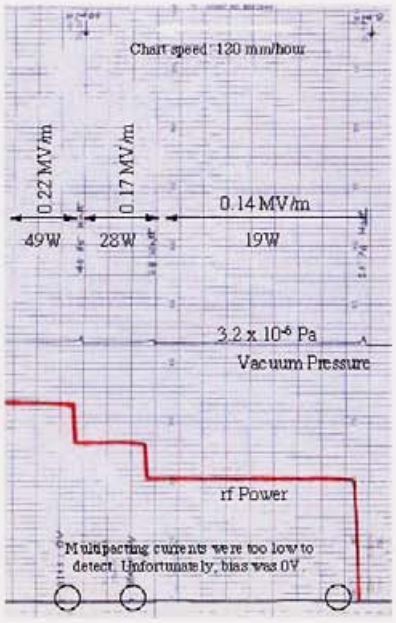

Figure 3.15: Multipacting incidents observed at room temperature during 1^{st} rf excitation before baking of the cavity (Part-1/4). Vacuum pressure, multipacting current, rf power inside cavity and peak electric field E_{pk} at inner conductor, respectively, are expressed in Pa, μA, Watt and MV/m.

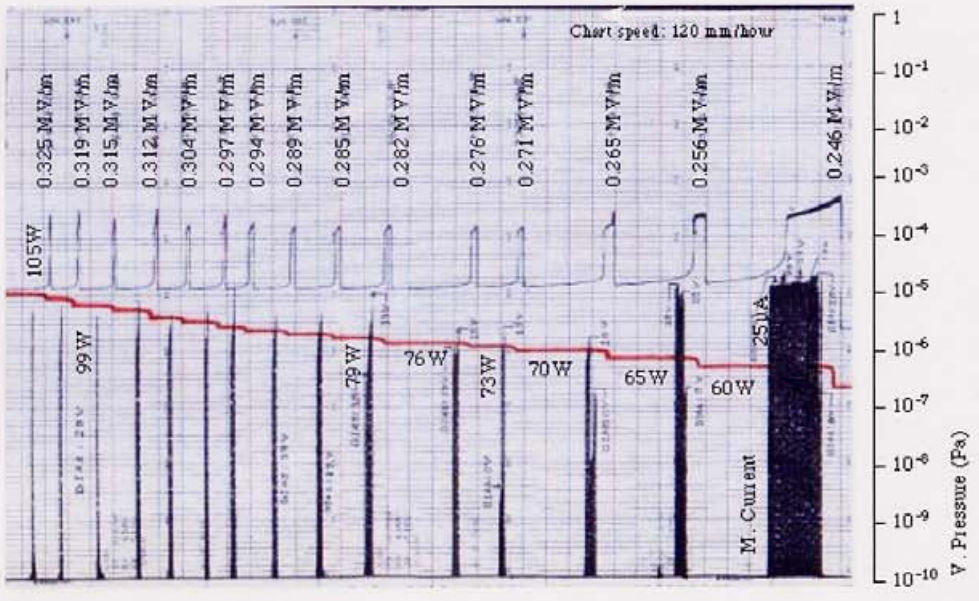

Figure 3.16: Multipacting incidents observed at room temperature during 1^{st} rf excitation before baking of the cavity (Part-2/4). Vacuum pressure, multipacting current, rf power inside cavity and peak electric field E_{pk} at inner conductor, respectively, are expressed in Pa, μA, Watt and MV/m.

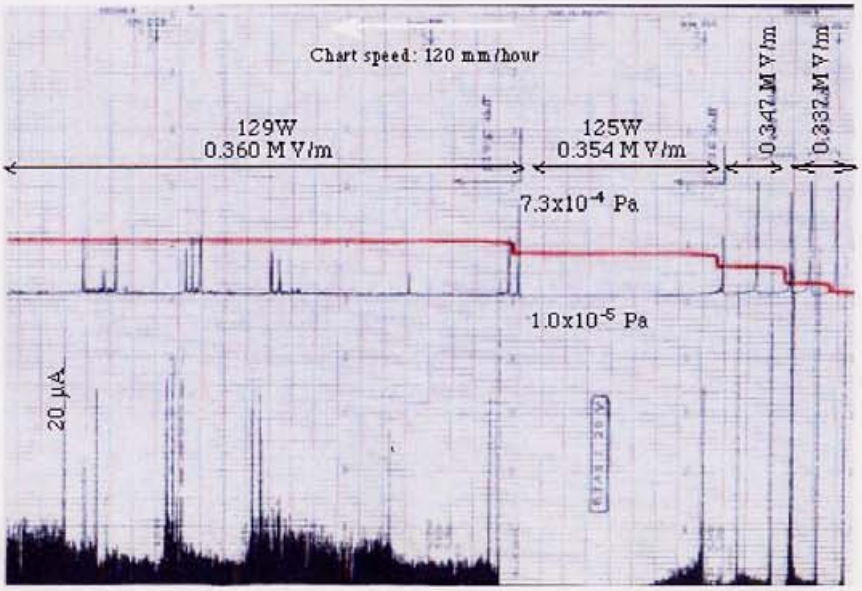

Figure 3.17: Multipacting incidents observed at room temperature during 1^{st} rf excitation before baking of the cavity (Part-3/4). Vacuum pressure, multipacting current, rf power inside cavity and peak electric field E_{pk} at inner conductor, respectively, are expressed in Pa, μA, Watt and MV/m.

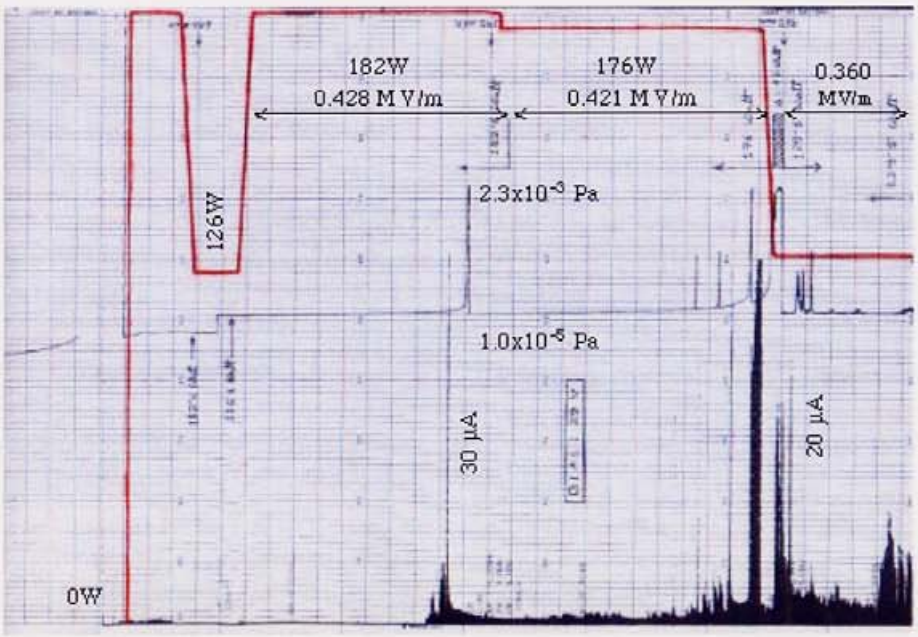

Figure 3.18: Multipacting incidents observed at room temperature during 1^{st} rf excitation before baking of the cavity (Part-4/4). Vacuum pressure, multipacting current, rf power inside cavity and peak electric field E_{pk} at inner conductor, respectively, are expressed in Pa, μA, Watt and MV/m.

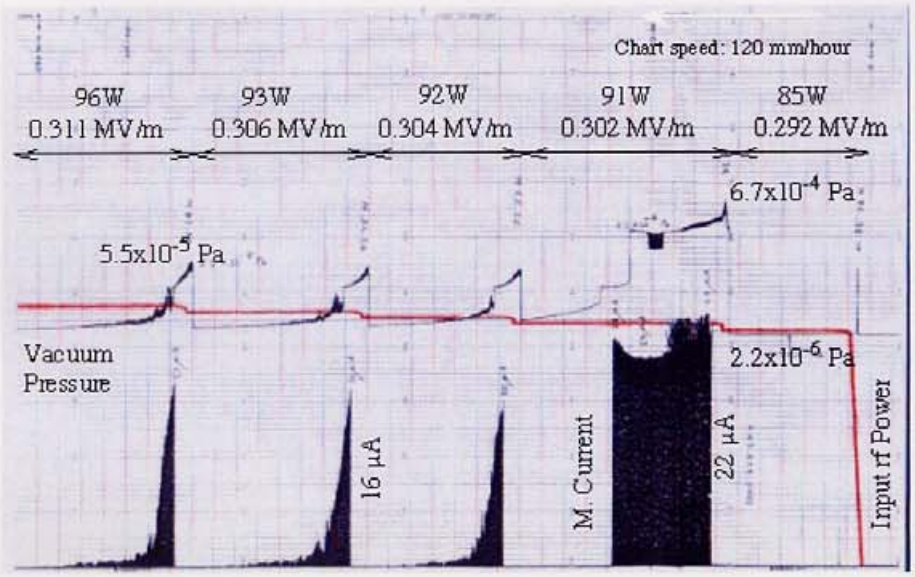

Figure 3.19: Multipacting incidents observed at room temperature during the 3^{rd} rf excitation before baking of the cavity (Part-1/3). Vacuum pressure, multipacting current, rf power inside cavity and peak electric field E_{pk} at inner conductor, respectively, are expressed in Pa, μA, Watt and MV/m.

After this rf excitation, we carried on the experiment without exposing the cavity to ambient air in order to study the change in multipacting phenomena during the subsequent rf excitations. We found that multipacting observed during the first rf excitation at lower rf power below 80W (284 kV/m), was not observed during the subsequent 2^{nd} and 3^{rd} rf excitation. But, there was no significant difference in multipacting incidents between the 2^{nd} and 3^{rd} rf excitation, although the interval between the two rf excitations was 20 days. Figures 3.19– 3.21 show the multipacting observed during the 3^{rd} rf excitation. A characteristic difference from the 1^{st} rf excitation was that the first multipacting incident was observed at relatively higher rf power between 80-90W and this incident was strong but very soft. Second incident took the longest time to become processed. Other multipacting incidents were observed more or less similar to that observed during the 1^{st} rf excitation.

Room temperature multipacting without baking can be summarized as follows:

- For input power below 60W (246 kV/m), there were a few multipacting incidents. These were very soft and weak as well. Once these incidents were processed, these multipacting will never occur until the cavity was exposed to ambient air.

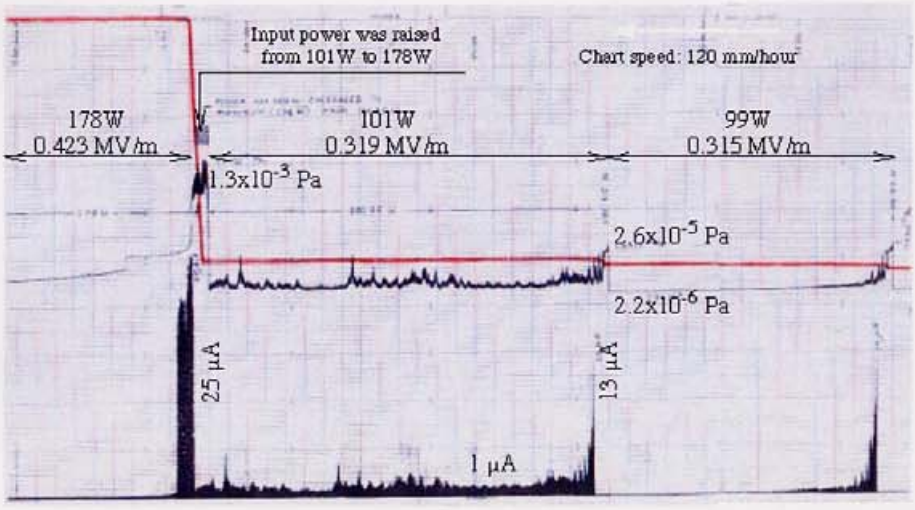

Figure 3.20: Multipacting incidents observed at room temperature during the 3^{rd} rf excitation before baking of the cavity (Part-2/3). Vacuum pressure, multipacting current, rf power inside cavity and peak electric field E_{pk} at inner conductor, respectively, are expressed in Pa, μA, Watt and MV/m.

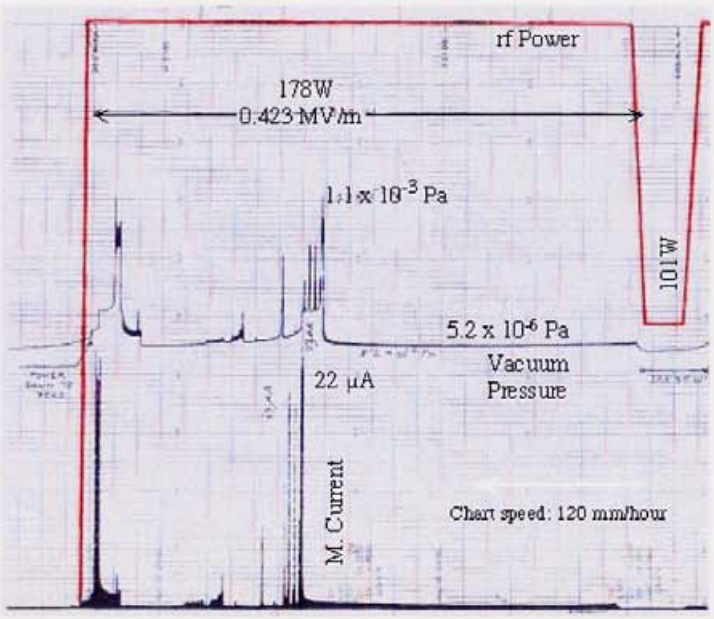

Figure 3.21: Multipacting incidents observed at room temperature during the 3^{rd} rf excitation before baking of the cavity (Part-3/3). Vacuum pressure, multipacting current, rf power inside cavity and peak electric field E_{pk} at inner conductor, respectively, are expressed in Pa, μA, Watt and MV/m.

- In the range 60 – 80W (246 – 284 kV/m), multipacting incidents were strong. First incident in this range took the longest time, around 15 minutes, to be processed. Once these multipacting were processed, these never happened until the cavity was exposed to ambient air.

- In the range 80 – 100W (284 – 317 kV/m), multipacting incidents were strong but soft. Within one minutes, these incidents became processed down. After processing of these multipacting, if the cavity was left without rf power for a few days, then these multipacting incidents, particularly around and above 90W, occurred during the following rf excitations, even if the cavity was not exposed to ambient air.

- Power above 100W (317 kV/m), multipacting becomes very severe. Strong incidents occurred irregularly against the background of continuous series of weak incidents. Our available input power (180W) was not enough to surmount this hard barrier.

After carrying out the multipacting experiments without baking, we baked the cavity at 100^0C for 40 hours in order to study the effect of baking on multipacting. Baking temperature was limited due to use of Indium seal at the joint between the outer and inner conductors. Figures 3.22 – 3.25 shows the multipacting incidents observed at room temperature after baking the cavity. Comparing with Figures3.19 – 3.21, we found that multipacting observed after baking seemed similar or somewhat more severe than the multipacting observed before baking the cavity. Although there was no symptom of alleviation of multipacting due to baking, we found that multipacting barrier above 100W became completely processed down after baking of the cavity. We also carried out the multipacting experiment after exposing the cavity to the ambient air and then preparing the vacuum with baking at 100^0C for 40 hours. Figure 3.26 shows the multipacting observed during the 1^{st} rf excitation. In this case too, multipacting above input power of 100W became eventually processed down. So, ***baking at 100^0C enabled us to process the multipacting, which did not become processed before baking of the cavity.***

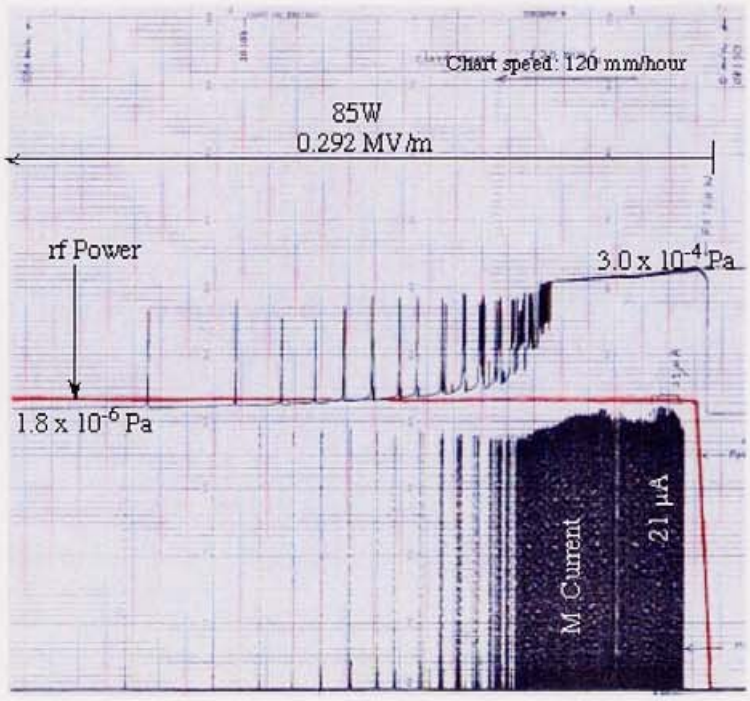

Figure 3.22: Multipacting incidents observed at room temperature after baking of the cavity (Part-1/4). Vacuum pressure, multipacting current, rf power inside cavity and peak electric field E_{pk} at inner conductor, respectively, are expressed in Pa, μA, Watt and MV/m.

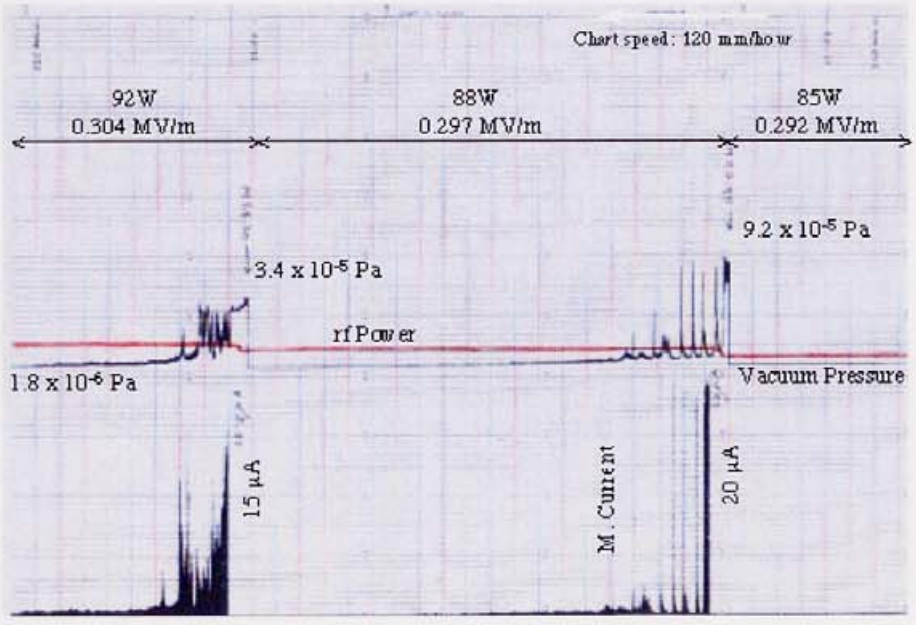

Figure 3.23: Multipacting incidents observed at room temperature after baking of the cavity (Part-2/4). Vacuum pressure, multipacting current, rf power inside cavity and peak electric field E_{pk} at inner conductor, respectively, are expressed in Pa, μA, Watt and MV/m.

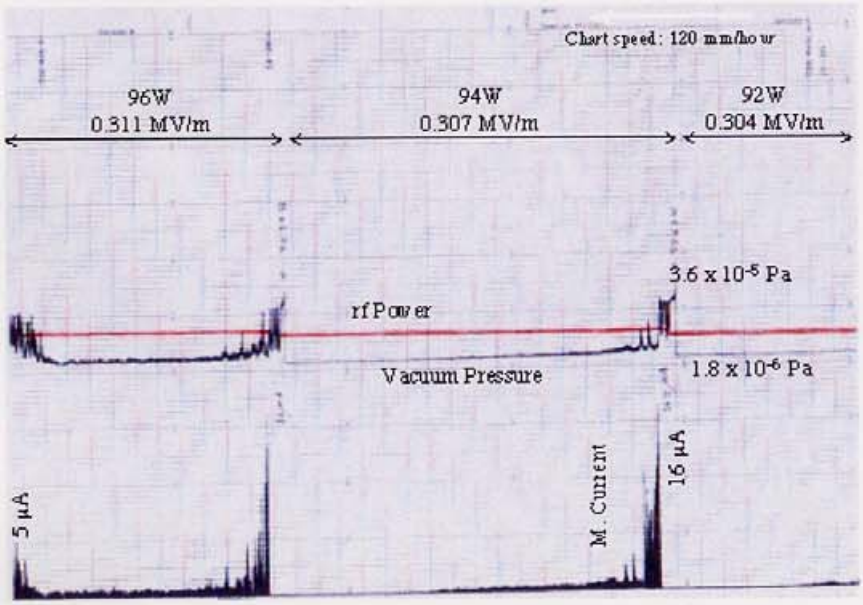

Figure 3.24: Multipacting incidents observed at room temperature after baking of the cavity (Part-3/4). Vacuum pressure, multipacting current, rf power inside cavity and peak electric field E_{pk} at inner conductor, respectively, are expressed in Pa, μA, Watt and MV/m.

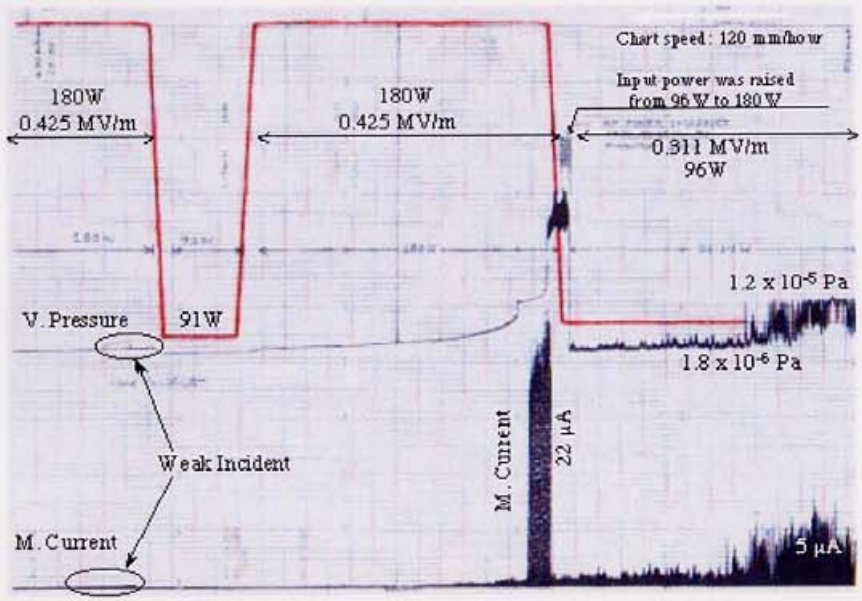

Figure 3.25: Multipacting incidents observed at room temperature after baking of the cavity (Part-4/4). Vacuum pressure, multipacting current, rf power inside cavity and peak electric field E_{pk} at inner conductor, respectively, are expressed in Pa, μA, Watt and MV/m.

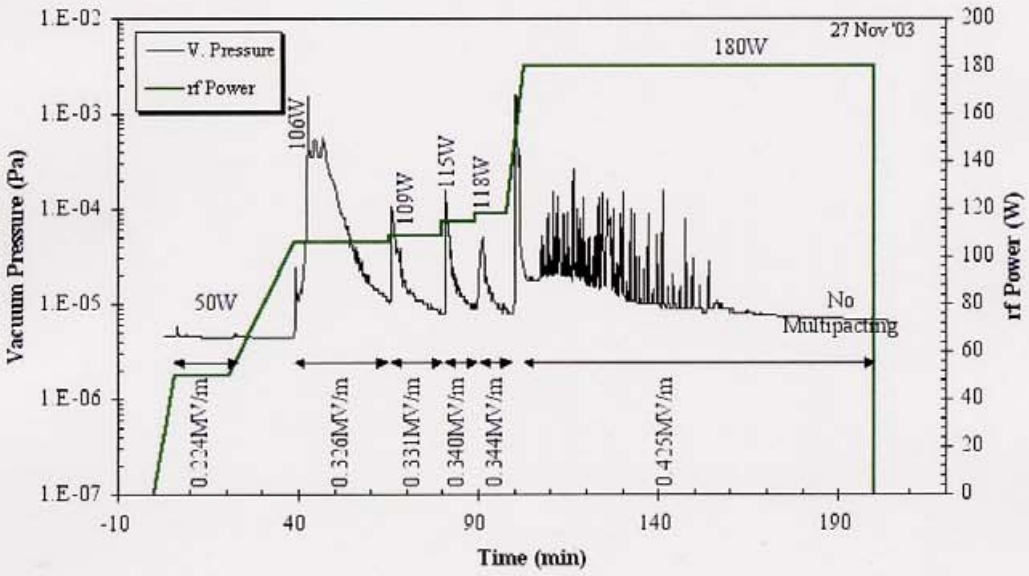

Figure 3.26: Multipacting incidents observed at room temperature during 1^{st} rf excitation after exposing the cavity to ambient air and then preparing vacuum with baking of the cavity. Vacuum pressure, multipacting current, rf power inside cavity and peak electric field E_{pk} at inner conductor, respectively, are expressed in Pa, μA, Watt and MV/m.

3.7.3 Multipacting at 4.2K without admission of any gas molecules

Figure 3.27 shows the multipacting observed after cool down the cavity at 4.2K. Comparing to the multipacting at room temperature, we found a few multipacting incidents at 4.2K. In the case of room temperature experiments, many multipacting incidents were observed below the peak electric field of 0.3MV/m and multipacting became very severe above this electric filed. On the contrary, at 4.2K no multipacting was observed below the peak electric filed of 0.3MV/m Moreover, power levels of multipacting were easily distinguishable. In our experiments, multipacting was observed typically at input power 43W (321 kV/m), 54W (360 kV/m), 77W (429 kV/m), 86W (454 kV/m), 104W (499 kV/m), 156W (611 kV/m), and 185W (666 kV/m). Multipacting at lower power levels were strong but soft; became processed within few minutes. Multipacting at higher power, particularly above 180W, was found weak. Sometimes, strong incidents were also observed along with the weak incidents. It took about half an hour to become processed; 95-100% of this processing time was due to the weak incidents.

Our experiments showed that ***cool down at 4.2K reduced the multipacting incidents but could not eliminate the multipacting***.

In our experiments at 4.2K, we observed that multipacting below input power of 100W (489 kV/m) seemed somewhat different than the multipacting above 100W. During the multipacting below 100W, for example at 54W and 74W in Figure 3.27, we observed the change in reflected and transmitted signal from the cavity into the unstable condition as shown in Figure 3.33. But, during the multipacting above 100W, for example at 104W, 156W and 165W in Figure 3.27, we did not observe any apparent change in reflected and transmitted signals. In these cases, multipacting incidents were identified only by the multipacting current.

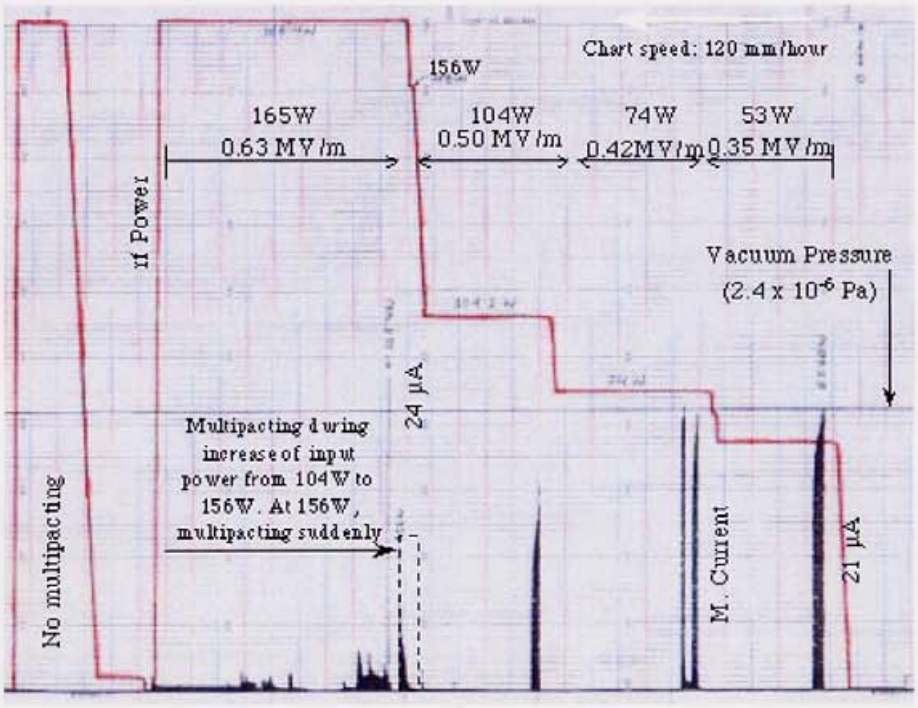

Figure 3.27: Multipacting incidents observed at 4.2K. Vacuum pressure, multipacting current, rf power inside cavity and peak electric field E_{pk} at inner conductor, respectively, are expressed in Pa, μA, Watt and MV/m.

3.7.4 Multipacting at 4.2K with H_2 molecules

It is generally believed that adsorbed H_2 molecules may be the main source of multipacting or enhance the multipacting. We tried to show experimentally that this was really so. If multipacting is observed after adsorption of H_2 molecules on a no-multipacting surface, then it can be concluded that H_2 molecules act as the source of multipacting. So, after processing all multipacting at 4.2K in the range of our power level, 5 x 10^{18} H_2 molecules were admitted into the cavity at 4.2K. This admission of H_2 changed the cavity vacuum [5] from 7.7 x 10^{-7} Pa to 5.7 x 10^{-5} Pa at 4.2K. From our adsorption-desorption experiment, we know that H_2 has saturation pressure of the order of 10^{-4} Pa at 4.2K. The vacuum pressure of 5.7 x 10^{-5} Pa indicated the formation of multilayer of H_2 molecules, although it was not saturated. Then cavity was excited with the rf power up to 200W. Surprisingly, there was no evidence of multipacting.

After this rf excitation, cavity was kept at 4.2K for 15 hours and then, additional 2.5 x 10^{18} H_2 molecules were admitted into the cavity to make the cavity saturated by H_2 at 4.2K. This admission of H_2 molecules changed the cavity vacuum pressure to 1.4 x 10^{-4} Pa. From our adsorption experiment, we learnt that this was the vacuum pressure of a H_2 saturated surface at 4.2K. But, this time also no evidence of multipacting was found.

This experimental result showed, contrary to the general belief, that ***H_2 molecule did not act as the source of multipacting***.

After having the surprising result - *H_2 was not the source of multipacting* - we conducted the experiments in various ways to confirm the result.

In our cavity, there was a 10 mm gap along the inner conductor. This gap made the entrance opening of the H_2 molecules from the H_2 feeding pipe as shown in Figure 3.28. Adsorption time of H_2 at 4.2K may be comparable to the experimental time. So, there might be a question whether the admitted H_2 molecules entered the cavity or remained trapped at the entrance and outside the cavity. Usually we used to wait few hours after the admission of H_2 and, particularly, we waited about 28 hours after admission of H_2 molecules in the above mentioned experiment. This time might be sufficient to make H_2 molecules entered the cavity, especially in the case of saturated pressure. Still being on the assumption of trapping of H_2 molecules outside the cavity, H_2 molecules were admitted into the cavity at 30^0C. Adsorption time of H_2 at 30^0C is order of 10^{-11} sec. So, very soon admitted H_2 uniformly distributes all over the surface. This ensured the formation of H_2 layers everywhere in side the cavity after cool down at 4.2K. Cavity vacuum was found to be 3.7 x 10^{-4} Pa at 4.2K.As our H_2 adsorption experiment revealed, this was the vacuum

[5]Cavity vacuum was measured at room temperature environment by using a Bayard-Alpert type ionization gauge as illustrated in Figure 3.28.

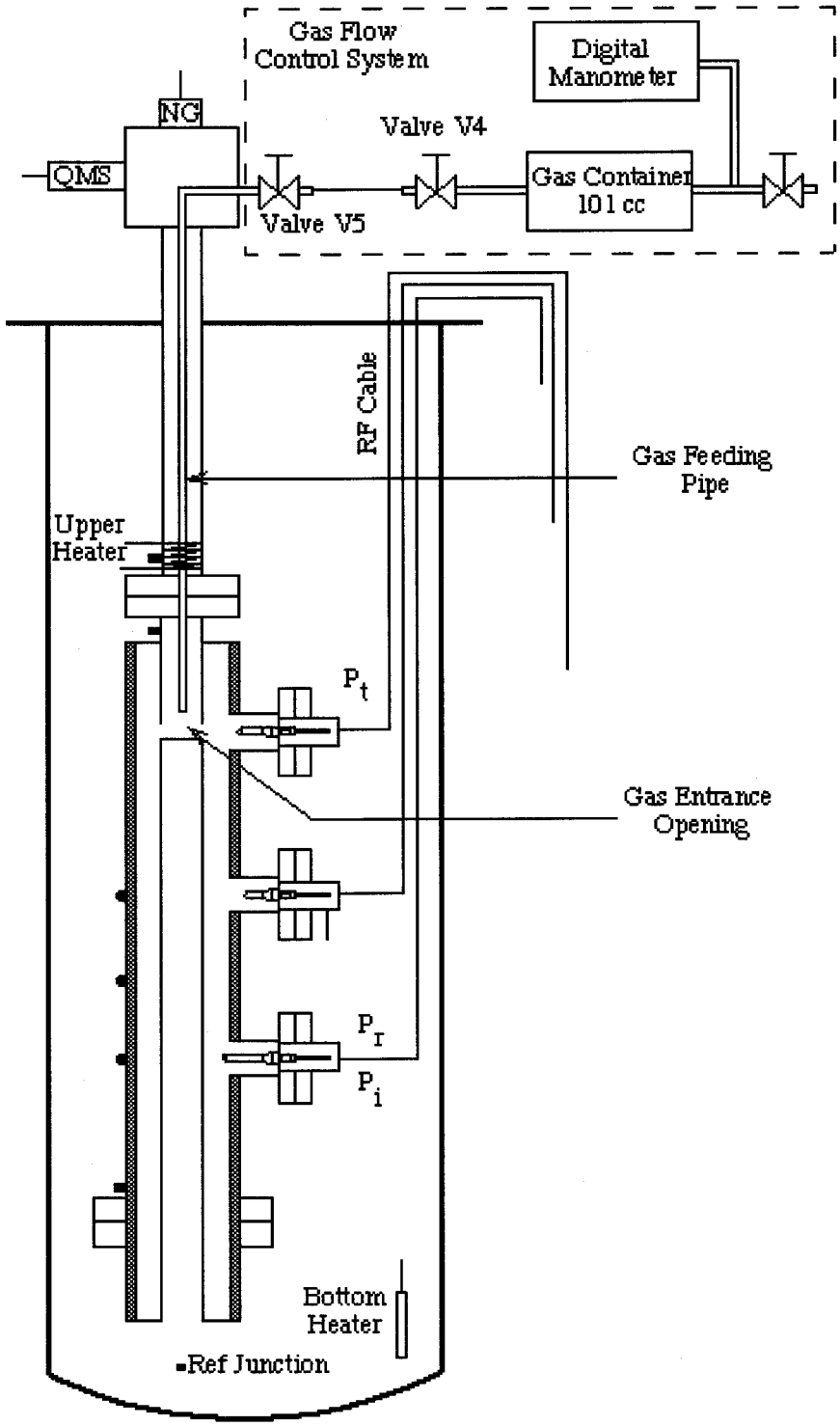

Figure 3.28: Schematic view of the setup of cryostat, vacuum gauges (NG & QMS) and gas flow control system.

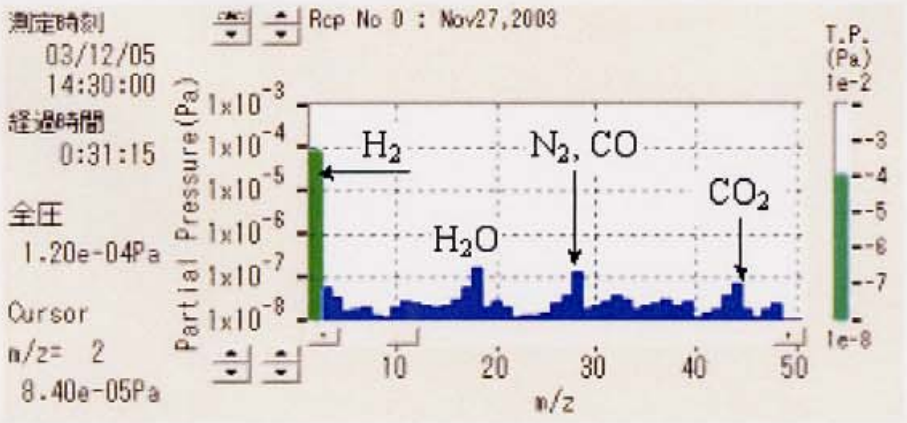

Figure 3.29: Partial pressure of residual gas molecules at 4.2K after becoming saturated by H_2 molecules.

pressure of a H_2 saturated surface at 4.2K. Figure 3.29 shows the vacuum state of the cavity at 4.2K after admission of H_2 molecules at 30°C. And, this was the vacuum state we always observed when the cavity became saturated by H_2 at 4.2K.

At this vacuum state, the cavity was excited by rf power up to 180W but no multipacting was observed.

As mentioned in §3.7.3, whenever the cavity was cooled down from room temperature without admission of any gas molecules, multipacting was observed. In the above experiment, cavity was cooled down after admission of H_2 molecules but no multipacting was observed. Therefore, *this experimental result not only revealed that* ***H_2 did not act as the source of multipacting*** *but also showed that* ***saturated H_2 surface suppressed the multipacting.***

Admission of H_2 at room temperature caused sudden increase of the vacuum pressure of the cavity. This sudden increase of vacuum pressure might cause the breakdown of vacuum gauges, particularly the nude gauge. So, in the case of admission at room temperature, we had to switch off the vacuum gauges. As a result, we had to loose vacuum data, particularly the base vacuum at 4.2K. So, in our experiment, we preferred to admit H_2 molecules after cool down at 4.2K. In order that the admitted H_2 molecules were not trapped outside the cavity, the connecting vacuum pipe was kept warm by using the upper heater wound around the lower part of the connecting vacuum pipe as shown in Figure 3.28.

In order to confirm that *saturated H_2 surface suppresses the multipacting*, we repeated the experiment with H_2 saturated surface but this time H_2 molecules were admitted after the cool down to 4.2K. Vacuum state was shown in the center part of Figure 3.30. Comparison

with Figure 3.29 reveals that the cavity became saturated by H_2 molecules at 4.2K. Same as previous experiments, ***no multipacting was observed.*** After rf excitation, the cavity was warmed up to 46K to desorb the H_2 molecules out of the cavity. Then the cavity was again cooled down to 4.2K. Cavity vacuum and partial pressure of H_2 were almost same as those we had before admission of H_2 at 4.2K as shown in Figure 3.30. So, the condition of inner surface of the cavity might be considered as before the admission of H_2 molecules. Now with rf excitation, multipacting was observed at input power 45W, 165W, 170W, 175W and maximum 195W. At higher powers 170W, 175W and 195W, multipacting incidents were very weak – very hard to detect in our setup. But, these multipacting incidents took more than 5 minutes to be processed.

In this experiment too, ***multipacting was not observed with the admission of H_2 molecules.*** But after the desorption of H_2 molecules, multipacting was observed. This confirmed that ***saturated H_2 surface suppressed the multipacting.***

We also carried out the experiments to find out the difference of *the multipacting suppression effect between multilayer and monolayer of H_2.* For this purpose, again the cavity was made saturated by H_2 molecules at 4.2K. This time too, no multipacting was observed with rf excitation up to 215W. Then keeping the metal angle valve between the vacuum pump and the coaxial cavity opened, cavity was warmed up at 6K to desorb some H_2 molecules out of the cavity. After cool down at 4.2K, cavity vacuum was reached at 3.1 x 10^{-5} Pa. Comparison of this vacuum pressure with the saturated pressure [6] showed that the cavity surface was covered with *the multilayer of H_2 molecules but not saturated.* At this state of the cavity vacuum, *no multipacting was observed* with the rf excitation.

Again, keeping the metal angle valve opened, the cavity was warmed up at 23K and then cooled down at 4.2K. This temperature was sufficient to desorb H_2 molecules even from the monolayer. So, after cool down at 4.2K, the cavity surface could be considered as almost same as the surface obtained after cool down at 4.2K from room temperature. But, the proportion of surface covered with H_2 molecules was certainly larger than that of the virgin surface, since some H_2 molecules might not have enough time to get out from the cavity. With rf excitation at this stage, strong multipacting was observed at input power 84W for less than 30 seconds. At input power around 190W, very weak multipacting was observed which took about 30 minutes to be processed.

Again, the cavity was warmed up at 30K by keeping the metal angle valve open and then cooled down at 4.2K. Now the cavity surface was less populated by H_2 molecules than the surface we had before warm up. At this stage, strong incidents were observed at 83W and 89W. Also very faint incidents were appeared at higher power 215W.

[6] Saturated pressure was recorded as 3.6 x 10^{-4} Pa.

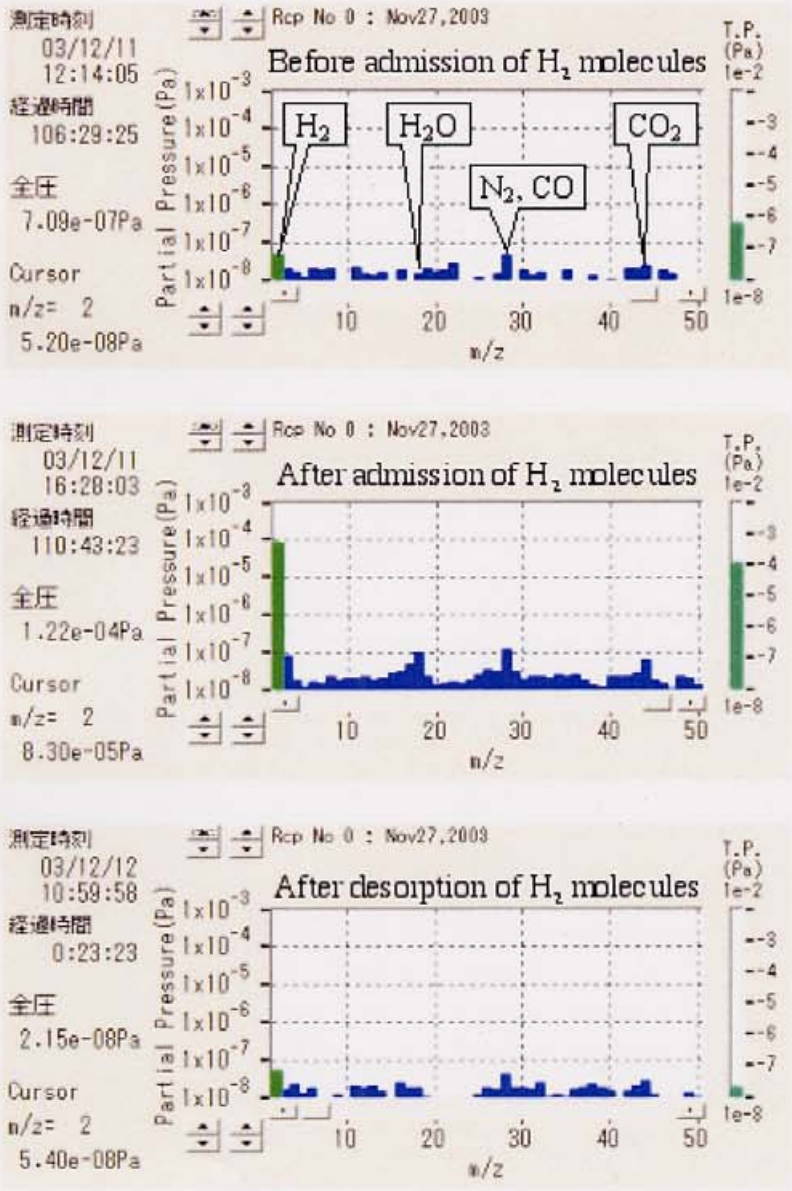

Figure 3.30: Partial pressure of residual gas molecules at 4.2K at different stages of the multipacting experiment with saturated surface of H_2 molecules.

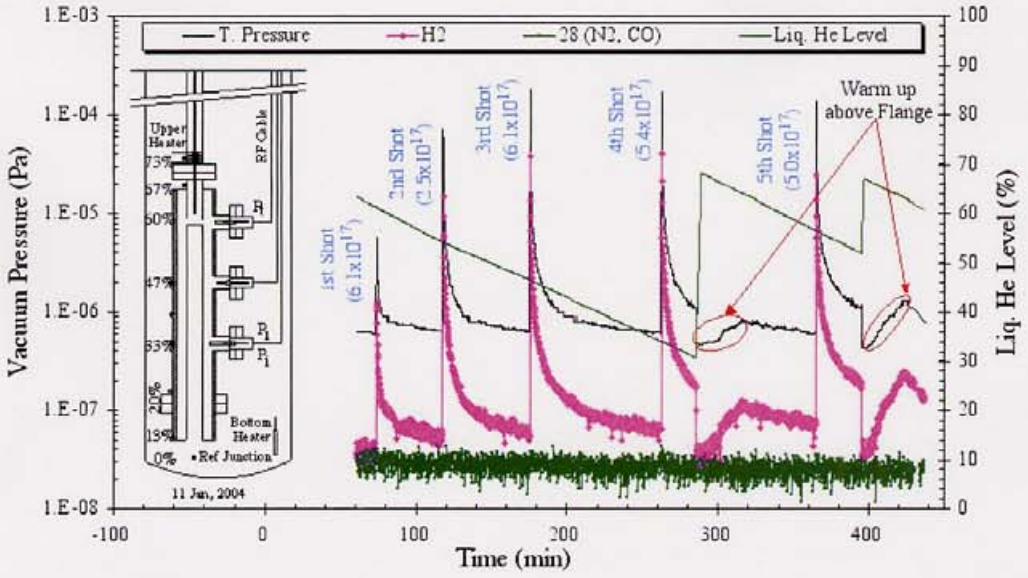

Figure 3.31: Admission of H_2 gas molecules into the cavity at 4.2K in order to form monolayer of H_2.

This experiment showed that ***not only saturated but also multilayer surface of H_2 suppressed the multipacting***. We also found that *multipacting incident increased with the decrease of population of H_2 molecules in the case of partial monolayer.*

In another experiment, we tried to deliberately make a uniform monolayer of H_2. In order to do so, H_2 molecules were admitted step by step into the cavity after cool down at 4.2K. Figure 3.31 illustrates how H_2 molecules were admitted into the cavity. Upper heater (5.3W) was kept ON since the cool down of the cavity so that the admitted H_2 molecules did not remain trapped out side the cavity. Moreover, liquid helium level in cryostat was always maintained to keep the cavity only sunk into the liquid helium. As shown in Figure 3.31, up to the 4^{th} shot of H_2 molecules the cavity vacuum attained the base value (6.2 x 10^{-7} Pa), which we had after cool down the cavity. But, after the 5^{th} shot of H_2 molecules, the vacuum pressure slightly increased to 8.0 x 10^{-7} Pa. This indicated that almost all H_2 molecules up to 4^{th} shot and maybe, some of the 5^{th} shot were directly adsorbed on the cavity surface to form a uniform monolayer. Rest molecules of the 5^{th} shot formed layer upon the monolayer so that the vacuum pressure increased from the base pressure. In this way, we formed a uniform monolayer and a partial layer of H_2 upon the monolayer. The number of H_2 molecules required to form these layers were 2.5 x 10^{18} molecules. This number was also satisfactory from the point of view of calculation. Geometrical surface [7] of the

[7] Geometrical surface of the cavity roughly equals to 1180 cm^2.

cavity requires 1.8 x 10^{18} H_2 molecules to form a uniform monolayer. After the admission of H_2 molecules, no multipacting was observed with the rf excitations up to input power 215W.

This experiment showed that ***a uniform monolayer of H_2 suppressed the multipacting.***

As mentioned before, we already studied the multipacting with the partial monolayer of H_2. In those cases, partial monolayer was formed by the desorption of H_2 molecules from the multilayer surface and so, the population of adsorbed H_2 molecules remained unknown. Those experiments indicted that multipacting incidents increased with the decrease of population of adsorbed H_2. We carried out more experiments to study comprehensively the multipacting with the partial monolayer. This time we deliberately made the partial monolayer by admitting a known amount of H_2 molecules.

Experiment - 1: In this experiment with partial monolayer of H_2, 5 x 10^{17} H_2 molecules were admitted into the cavity after cool down at 4.2K. After admission of H_2 molecules, there was no change in either the total vacuum pressure (4.9 x 10^{-7} Pa) or the partial pressure (3.0 x 10^{-8} Pa) of H_2. This indicated that all admitted H_2 molecules directly adsorbed on the cavity surface and formed a partial monolayer of H_2. After admission of H_2 molecules, only one incident was observed at input power 50W. There was no faint incident, very often observed at higher input power.

After rf excitation, in order to reorganize the adsorption sites of the partial monolayer, the cavity was warmed up to 41K by keeping the metal angle valve closed. This temperature was enough to desorb H_2 molecules from the monolayer, but H_2 molecules could not go out of the cavity because of keeping the metal angle valve closed. Then the cavity was cooled down at 4.2K. Upper heater (5.3W) was kept ON since the start of warm up of the cavity and switched OFF after 2 hours of cool down the cavity so that the H_2 molecules, contained inside the connecting vacuum pipe, entered into the cavity and adsorbed on the cavity surface. After cool down at 4.2K, the cavity vacuum and the partial pressure of H_2 were almost same as those we had before warm up the cavity. At this stage, ***no multipacting was observed*** with the rf excitation up to input power of 215W.

Experiment - 2: In this experiment with partial monolayer, 1.1 x 10^{18} H_2 molecules were admitted into the cavity after cool down to 4.2K. After admission of H_2 molecules, there was no change in either the total vacuum pressure (3.8 x 10^{-7} Pa) or the partial pressure (3.2 x 10^{-8} Pa) of H_2. This indicated that all admitted H_2 molecules directly adsorbed on the cavity surface and formed a partial monolayer of H_2. But, density of population of H_2 was larger than twice the density, which we obtained in the Experiment - 1. At this stage

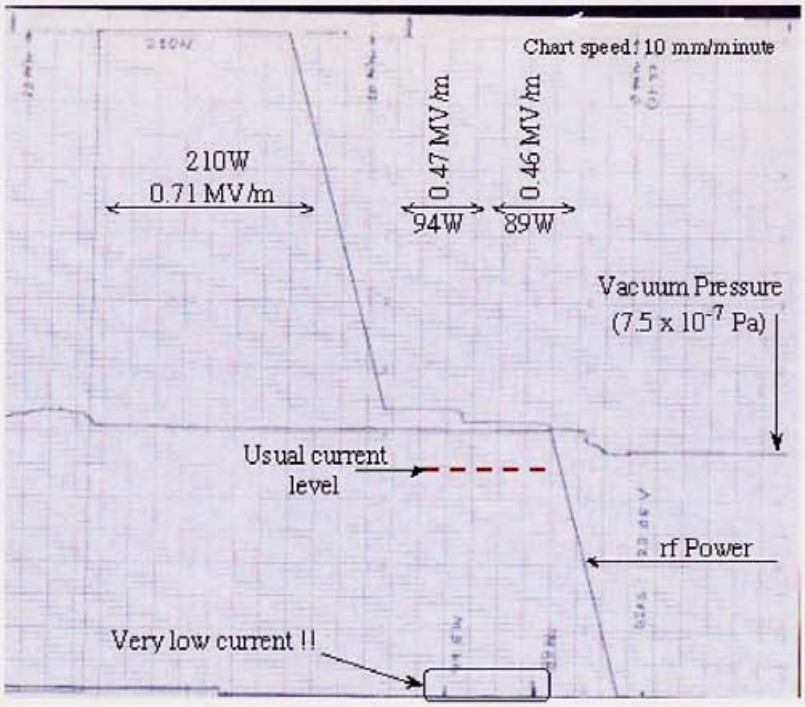

Figure 3.32: Multipacting incidents observed with partial monolayer of H_2 molecules at 4.2K.

too, ***no multipacting was observed***.

After the rf excitation, cavity was warmed up to 57K to desorb the admitted H_2 molecules out of the cavity. After cool down at 4.2K, multipacting was observed at 78W, 80W, 83W and 89W. All these multipacting incidents were strong but soft; became processed within around 15 seconds.

Experiment - 3: This time too 1.1 x 10^{18} H_2 molecules (same as Experiment - 2) were admitted into the cavity after cool down the cavity at 4.2K. This time multipacting was observed at input power 89W and 94W. But, as illustrated in Figure 3.32, these multipacting incidents were very weak; peak current due to multipacting electrons was about 1 μA whereas the usual current levels were above 10 μA in our measuring setup. This might be explained that multipacting sites were far away from the current measuring port.

All these experimental results of partial monolayer may be explained as follows. If all the multipacting sites are covered by the H_2, then no multipacting occurs. With the partial monolayer built up from the same number of H_2 molecules, once no multipacting was observed because all probable multipacting sites were covered by the monolayer. In other

case, multipacting was observed with much less current because nearby multipacting sites around the current measuring port were covered with the monolayer but far away multipacting sites were not covered by H_2 layer. In the case of formation of partial monolayer with less amount of H_2 molecules, probability of bare multipacting sites was larger and so, multipacting was observed. After cool down the cavity at 4.2K from room temperature, without admission of H_2 molecules, only residual H_2 gas molecules built up the least populated monolayer. So, the probability of bared multipacting sites was largest. This was the reason, always multipacting was observed after cool down the cavity without admission of H_2 molecules.

With this explanation on monolayer multipacting, it could be concluded that ***H_2 molecule suppressed the multipacting***.

3.7.5 Multipacting at 4.2K with CO

In ultra high vacuum, after H_2 dominant residual gas molecule is CO. In contrast to H_2 molecule, CO is a polar molecule like H_2O whereas latter molecule was found to enhance multipacting [22]. How is about CO?

In order to study the effect of CO on multipacting, after cool down the cavity at 4.2K, about 6 x 10^{19} CO molecules were admitted into the cavity. But there was no change in the cavity vacuum (7.5 x 10^{-7} Pa) and even in the partial pressure ($\sim 10^{-8}$ Pa) of CO after admission of CO. With the rf excitation up to input power of 200W, multipacting incidents were observed at input power 45W and 185W. Without admission of any molecules, multipacting was also observed at these power levels with the same order of multipacting current.

Being suspicious that the admitted CO molecules were trapped outside the cavity, the cavity was warmed up at 210K with keeping the vacuum pumping OFF. From our adsorption desorption experiment, we have learnt that 200K was enough to desorb out all dominant residual molecules, even H_2O started to desorb. At 210K, additional 5.1 x 10^{19} CO molecules were admitted into the cavity. So, in total 1 x 10^{20} CO molecules were moving inside the cavity. After cool down the cavity to 4.2K, the cavity vacuum was 1.0 x 10^{-6} Pa and the partial pressure of CO (and N2) was of the order of 10^{-8} Pa. With rf excitation, multipacting was observed at 85W and 87W. These incidents were also observed without admission of any gas molecules.

Multipacting incidents with the admission of CO were the same as those observed without admission of CO. Since admission of CO did not enhance the multipacting, it can be concluded that ***CO too did not act as the seed of multipacting***.

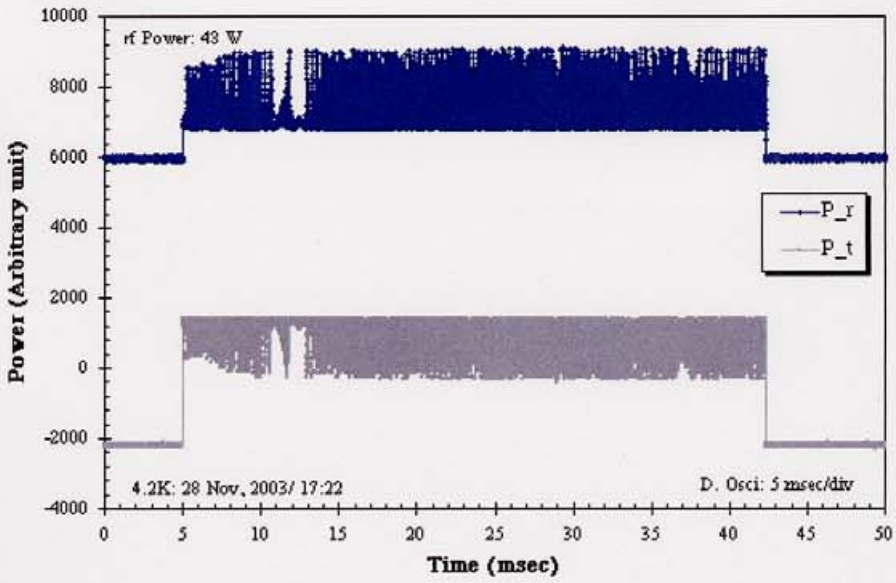

Figure 3.33: Time structure of reflected and transmitted signals during multipacting.

3.8 Time Structure of Multipacting

In our experiments, the coaxial cavity was driven by rf pulses of frequency 1 Hz and duty 3.6%. So, the cavity could store the available maximum rf energy only for 36 msec in each second. Therefore, if there was onset of multipacting, it could continue only for the 36 msec in each second. As a result, the multipacting current appeared as the series of spikes in the pen recorder chart. In order to study what happened in this 36 msec during multipacting, time structure of multipacting current was recorded in the digital oscilloscope along with the reflected and transmitted signal. Figure 3.33 shows the time structure of reflected and transmitted signal during multipacting in our experiments. After start of multipacting, how it continues? In order to find out this answer, we studied the development of multipacting in microsecond scale. Figure 3.34 shows multipacting incidents in microsecond scale. Obviously, multipacting did not occur continuously for the whole rf ON period. Rather multipacting originated, then became ceased and again, re-originated. In this way, multipacting continued until the multipacting became processed. The cease of multipacting can be explained as follows. Multipacting electron interacted with the rf field inside the cavity and thus, extracted the stored energy of the cavity. As a result, rf field level decreased with the development of multipacting and finally, became too low for the multipacting. This was the reason for the cease of multipacting. After the cease of multipacting, cavity restored its energy. But, as soon as the cavity restored its energy, multipacting did not observed to occur again. It needed some time to re-originate the multipacting. Sometimes, multipacting was observed to occur only for a fraction of each rf ON

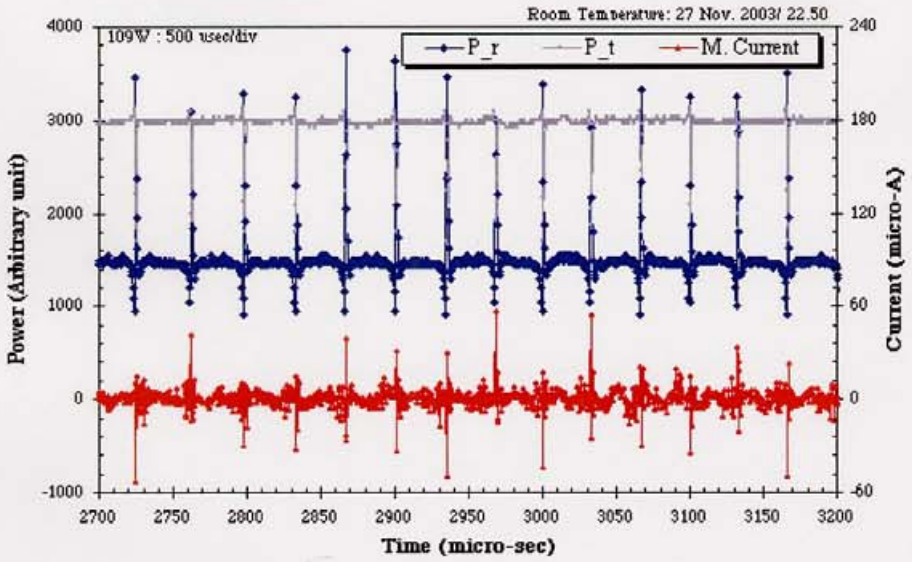

Figure 3.34: Microscopic view of multipacting incidents.

period (36 msec). For example, multipacting was observed around the 5^{th} msec of the rf ON period, no multipacting was observed during rest of the rf ON period.

Figure 3.35 illustrates the development of multipacting current. Multipacting current at first increased very slowly and then suddenly reached to maximum, where multipacting became ceased due to insufficient rf field. After initiation, multipacting sustained for a time of a few thousands of rf period. After the cease of multipacting, oscillation in multipacting current was, maybe, the noise attributed to the impedance mismatch of our current measuring circuit.

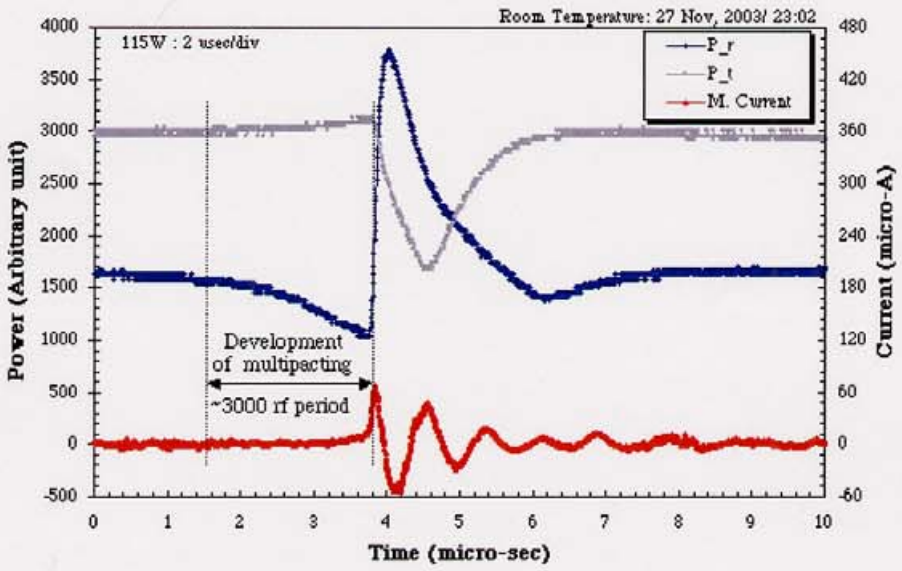

Figure 3.35: Development of multipacting.

Chapter 4

Conclusion

Objective of our experiment is to search out the seed of multipacting. There is a common speculation that adsorption of molecules on cooled surface enhances the multipacting. Usually the cavity is prepared with ultra-high vacuum where H_2 is the main dominant residual molecules. This leads our curiosity on H_2. So, before rf experiments with H_2, we studied the adsorption and desorption phenomena of H_2 at 4.2K.

From the study of adsorption of H_2 molecules at 4.2K on copper surface we have learnt how the vacuum pressure increases with the increase of amount of adsorbed H_2 molecules. At 4.2K, H_2 has a saturation pressure of the order of 10-4 Pa. Desorption of H_2 as a function of temperature can be characterized by a sharp peak followed by a broad peak. Sharp peak is due to desorption of the H_2 molecules, which are adsorbed on each other by the cohesive force between themselves. Position of the sharp peak is at around 5.6K. This gives us a measure of binding energy (0.48 mev) due to cohesive force between the H_2 molecules. On the contrary, the large peak is due to desorption of those H_2 molecules, which are adsorbed directly on the copper surface by the adhesive force. Position of the large peak is at around 14K. This yields a measure of binding energy of the adhesive force (1.2 mev) between copper and H_2 molecules.

For the study of multipacting, we made a coaxial cavity of copper. Main feature of our design is the selection of the excitation mode so that different cutting parts of the coaxial cavity are at the position where rf surface current is zero. This mode selection provided us to fabricate the coaxial cavity of rather high Q_0 (7000 at 20^0C) from copper. At input power 200W, peak electric field at inner conductor of our cavity is 0.45 MV/m at 25^0C and 0.69 MV/m at 4.2K. Field level of our cavity is higher than that of the input coupler of KEKB superconducting accelerating cavity.

In the case of room temperature (~25^0C), multipacting can occur at very low rf field – as low as 0.1 MV/m for the peak electric field[1]. But, multipacting becomes severe above the peak electric field of 0.3 MV/m. This multipacting has not become processed although the input power has been raised to the peak electric field 0.4 MV/m. After baking of the cavity at 100^0C for 40 hours, multipacting levels have been found almost same as those observed before baking. However, after baking, multipacting observed above the peak electric field of 0.3 MV/m has become processed down. We also have found that after processing of the multipacting observed below the peak electric field of 0.28 MV/m, these multipacting incidents do not occur during the subsequent rf excitations, if the cavity is not exposed to ambient air. Multipacting above the peak electric field of 0.28 MV/m occurs during every rf excitation, even if the cavity is not exposed to ambient air.

After cool down the cavity at 4.2K, we have observed much less multipacting incidents. It requires rather high field – as high as 0.32 MV/m for the peak electric field, to occur the first multipacting incident. At 4.2K, no severe multipacting like room temperature multipacting has been observed. All multipacting incidents have become processed within a few minutes. Only exception is the very weak multipacting observed above the peak electric field of 0.65 MV/m; it requires about half an hour to become processed. Once processed, multipacting does not occur if the cavity is kept at 4.2K.

We have studied the multipacting with adsorption of H_2 molecules. We have found that adsorbed H_2 does not act as the seed of multipacting, rather suppresses the multipacting. From the complete monolayer to saturated surface of H_2, we have never observed any multipacting at 4.2K. In case of partial monolayer, sometimes multipacting has been observed and sometimes not. Reason of this observance can be explained as follows. If the multipacting sites are covered by the H_2 layer, then multipacting is not observed. With the increase of population of adsorbed H_2 molecules, probability of bared multipacting sites and number as well decrease and approach to zero as the population makes a complete monolayer of adsorbed H_2. This argument also explains why multipacting was always observed in our experiment without admission of H_2 molecules. In this case, residual H_2 gas molecules build up the least populated monolayer of adsorbed H_2 and so, this increases the probability of bared multipacting sites and number as well.

After chasing the H_2, we also have studied the multipacting with adsorption of CO molecules at 4.2K. With the adsorption of CO, We have found the same multipacting as that observed after cool down the cavity at 4.2K from room temperature. Since adsorption of CO does not enhance the multipacting, it can be concluded that adsorbed CO does not act as the seed of multipacting.

[1]Here, peak electric field always refers to the field at the inner conductor of the coaxial cavity

At room temperature, baking at 100^0C has enabled us to process the multipacting barrier above the peak electric field 0.3 MV/m. This indicates that adsorbed H_2O may act as the seed of multipacting.

We have also studied the development of multipacting. After generation of multipacting, it becomes ceased due to fall of stored energy of the cavity and again, originates after the cavity restores its energy. In this way, multipacting continues until process down. We have found that after the cease of multipacting, it does not restart as soon as the cavity restores its energy. It seems that multipacting needs some kind of triggering to occur.

Appendix A

Analytical Calculation of Cavity Parameters

Due to cylindrical symmetry, cylindrical coordinate (r, ϕ, z) was adopted, as shown in Figure A.1, for the analytical calculation. Origin was taken at the middle of symmetrical axis.

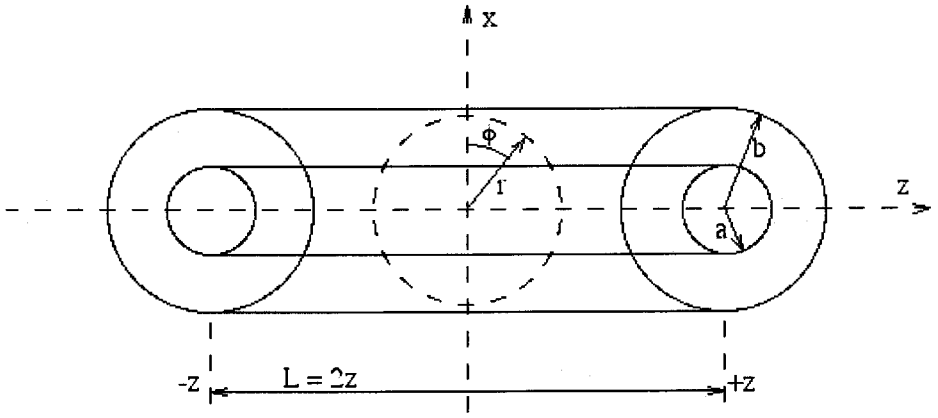

Figure A.1: Coordinates for the coaxial cavity.

A.1 Fields inside the coaxial cavity

TEM modes propagating along z-axis form standing wave due to reflection at the both ends of the cavity. Due to cylindrical symmetry, there is only radial component of electric filed and associated azimuthal magnetic field.

Electric Field:

$$\begin{aligned} E_z &= 0 \\ E_\phi &= 0 \\ E_r &= Z_0 \frac{I_0}{2\pi r} \langle e^{-\gamma z + j\omega t} + |\Gamma| e^{-\gamma^* z + j\omega t} \rangle \\ &= Z_0 \frac{I_0}{2\pi r} e^{j\omega t} \langle e^{-j\beta z} + e^{+j\beta z} \rangle \\ &= Z_0 \frac{I_0}{2\pi r} e^{j\omega t} 2\cos\beta z \\ &= Z_0 \frac{I_0}{\pi r} \cos\beta z \, e^{j\omega t} \end{aligned} \tag{A.1}$$

Magnetic Field:

$$\begin{aligned} H_z &= 0 \\ H_r &= 0 \\ H_\phi &= \frac{I_0}{2\pi r} \langle e^{-\gamma z + j\omega t} - |\Gamma| e^{-\gamma^* z + j\omega t} \rangle \\ &= j\frac{I_0}{\pi r} \sin\beta z \, e^{j\omega t} \end{aligned} \tag{A.2}$$

Here, γ is propagation constant defined as $\gamma = \alpha + j\beta$. For air, attenuation constant $\alpha \approx 0$. β is phase constant defined as $\beta = 2\pi/\lambda$. Γ is reflection coefficient and for perfect conductor $|\Gamma| = 1$. Z_0 is intrinsic impedance of the medium inside the cavity and $Z_0 = 377\ \Omega$ for air.

At the both ends ($z = \pm\frac{L}{2}$) of the cavity electric field must be zero (or minimum). This condition yields that allowed resonant wave length is given by

$$\lambda_N = \frac{2L}{N}; \qquad N = 0, 1, 2, \ldots, \textit{any positive integers} \tag{A.3}$$

$N = 0:$ $\lambda_0 = \infty$: $f_0 = 0$ *Static Field*
$N = 1:$ $\lambda_1 = 2L$ *Lowest Mode*
$N = 2:$ $\lambda_2 = L$
$N = 3:$ $\lambda_3 = 2L/3$
$N = 4:$ $\lambda_4 = L/2$ *Designed Mode*

In the design of coaxial cavity, we chose $N = 4$ as designed mode of excitation. So, our coaxial cavity was designed to excite at resonant wavelength of $\lambda = L/2$, where L is the length of the cavity.

A.2 Unloaded Quality (Q_0)

Unloaded quality Q_0 of a cavity is defined by

$$Q_0 = \omega \frac{U}{P_{loss}} \tag{A.4}$$

Here, U is the total energy stored in the cavity, P_{loss} is the power loss through the surface of the cavity and $\omega = 2\pi f$ is the resonant angular frequency.

In an electro-magnetic field, time averaged electric energy ($\overline{U}_e$) is equal to time averaged magnetic energy ($\overline{U}_m$) and so, the total electromagnetic energy(U) is twice of either electric or magnetic energy.

$$\begin{aligned} U &= 2\overline{U}_m \\ &= 2\,\frac{1}{4}\mu_0 \int_v |\vec{H}(\vec{r})|^2 dv \\ &= \frac{1}{2}\mu_0 \int_v |\vec{H}(\vec{r})|^2 dv \end{aligned} \tag{A.5}$$

Time averaged power loss through surface resistance R_s is given by

$$P_{loss} = \frac{1}{2} R_s \int_{surface} |\vec{H}_t(\vec{r})|^2 ds \tag{A.6}$$

So, the expression for Q_0 becomes,

$$Q_0 = \frac{2}{\delta_s} \frac{\int_v |\vec{H}(\vec{r})|^2 dv}{\int_{surface} |\vec{H}_t(\vec{r})|^2 ds} \tag{A.7}$$

where, $R_s = \frac{1}{\sigma \delta_s}$ and $\delta_s = \sqrt{\frac{2}{\omega \mu \sigma}}$

Here, σ and μ, respectively, are conductivity and magnetic permeability constant of the material of cavity. In more conventional form, Q_0 is given by

$$Q_0 \frac{\delta_s}{\lambda} = \frac{2}{\lambda} \frac{\int_v |\vec{H}(\vec{r})|^2 dv}{\int_{surface} |\vec{H}_t(\vec{r})|^2 ds} \tag{A.8}$$

where, λ is the resonant wavelength of the cavity.

From Eq(A.2), we find that

$$\begin{aligned}
\vec{H}(\vec{r}) &= \hat{e}_\phi \, \vec{H}_\phi(r,z) \\
&= \hat{e}_\phi \, j\frac{I_0}{\pi r} \sin(\beta_N z) \\
|\vec{H}(\vec{r})|^2 &= |\vec{H}(\vec{r}).\vec{H}^*(\vec{r})| \\
&= \frac{I_0^2}{\pi^2 r^2} \sin^2(\beta_N z) \\
\int_v |\vec{H}(\vec{r})|^2 \, dv &= \int_r \int_\phi \int_z \frac{I_0^2}{\pi^2 r^2} \sin^2(\beta_N z) \, r \, dr \, d\phi \, dz \\
&= \frac{I_0^2}{\pi^2} \int_a^b \frac{1}{r} dr \int_0^{2\pi} d\phi \int_{-L/2}^{+L/2} \sin^2(\beta_N z) dz \\
&= \frac{I_0^2}{\pi^2} \ln(\frac{b}{a}) \, 2\pi \, \frac{L}{2} \\
&= \frac{I_0^2}{\pi} L \ln(\frac{b}{a})
\end{aligned} \tag{A.9}$$

$$\int_{surface} |\vec{H}_t(\vec{r})|^2 ds$$

$$= 2 \int_{End\ Caps}^{z=\pm L/2} |\vec{H}_\phi(\vec{r})|^2 \, ds + \int_{Inner\ conductor}^{r=a} |\vec{H}_\phi(\vec{r})|^2 \, ds + \int_{Outer\ Conductor}^{r=b} |\vec{H}_\phi(\vec{r})|^2 ds$$

$$= 2\int_a^b \frac{I_0^2}{\pi^2 r^2}\sin^2(\beta_N\frac{L}{2})\,2\pi r\,dr \;+\; \int_{-L/2}^{+L/2}\frac{I_0^2}{\pi^2 a^2}\sin^2(\beta_N z)\,2\pi a\,dz + \int_{-L/2}^{+L/2}\frac{I_0^2}{\pi^2 b^2}\sin^2(\beta_N z)\,2\pi b\,dz$$

$$= \frac{4I_0^2}{\pi}\int_a^b \frac{1}{r}\,dr \;+\; \frac{2I_0^2}{\pi}(\frac{1}{a}+\frac{1}{b})\int_{-L/2}^{+L/2}\sin^2(\beta_N z)\,dz$$

[By boundary condition, $\sin^2(\pm\beta_N\frac{L}{2}) = 1$]

$$= \frac{4I_0^2}{\pi}\ln(\frac{b}{a}) \;+\; \frac{2I_0^2}{\pi}(\frac{1}{a}+\frac{1}{b})\frac{L}{2}$$

$$= \frac{I_0^2}{\pi}\left[4\ln(\frac{b}{a}) \;+\; L(\frac{1}{a}+\frac{1}{b})\right] \tag{A.10}$$

Using these expressions in Eq(A.7), we get

$$\begin{aligned} Q_0 &= \frac{2}{\delta_s}\frac{\frac{I_0^2}{\pi}L\ln(\frac{b}{a})}{\frac{I_0^2}{\pi}\left[4\ln(\frac{b}{a}) + L(\frac{1}{a}+\frac{1}{b})\right]} \\ &= \frac{2}{\delta_s}\frac{1}{\frac{4}{L}+\frac{\frac{1}{a}+\frac{1}{b}}{\ln\frac{b}{a}}} \\ &= \frac{1}{\delta_s}\frac{1}{\frac{2}{L}+\frac{1}{2b}\frac{1+\frac{b}{a}}{\ln\frac{b}{a}}} \end{aligned} \tag{A.11}$$

A.3 Relation between E_r and Q_0

Substituting Eq(A.9) into Eq(A.5), we get the total stored energy in the cavity:

$$U = \frac{\mu_0 I_0}{2\pi}L\ln(\frac{b}{a}) \tag{A.12}$$

In non-transient state, input rf power P to the cavity must be equal to total power loss P_{loss}. So, by inserting expression for U from Eq(A.4) into Eq(A.12), we get:

$$I_0^2 = \frac{PQ_0}{\mu_0 f L \ln(\frac{b}{a})} \tag{A.13}$$

With this expression, the Eq(A.1) becomes

$$E_r = Z_0 \frac{1}{\pi r}\sqrt{\frac{PQ_0}{\mu_0 f L \ln(\frac{b}{a})}} \cos(\beta z)\, e^{j\omega t} \tag{A.14}$$

$$E_{r,\,max} = Z_0 \frac{1}{\pi r}\sqrt{\frac{PQ_0}{\mu_0 f L \ln(\frac{b}{a})}} \tag{A.15}$$

Bibliography

[1] H. Piel, Proc. CERN Accelerator School: Superconductivity in Particle Accelerators, p 149-196, Hamburg 1988, Ed. S. Turner, CERN Report 89-04.

[2] Jens Knobloch, Ph.D. Thesis: Advanced thermometry studies of superconducting RF cavities, Cornell University, 1997.

[3] D. Proch et al., Proc. of the 1995 Particle Acclerator Conference, Dallas, USA. p. 1776-1778.

[4] C.M. Lyneis, H.A. Schwettman and J.P. Turneaure, Appl. Phys. Lett. 31, 541 (1977).

[5] V. Lagomarsino, G. Manuzio, R. Parodi, R. Vaccarone, IEEE Trans. MAG-15, 25 (1979).

[6] U. Klein and D. Proch, Proc. of the Conf. on Future Possibilities for Electron Acc, Charlottesville, p. N1-17, 1979, Ed. J.S. McCarthy and R.R. Whitney.

[7] P. Kneisel, R. Vincon and J. Halbritter, Nucl. Instr. Meth. 188, 669 (1981).

[8] W. Weingarten, Proc. of 2^{nd} Workshop on RF Superconductivity, p. 551-582, CERN, Geneva, Switzerland, 1984, Ed. H. Lengeler.

[9] K. Saito et al., Proc. Proc. of 7^{th} Workshop on RF Superconductivity, p. 379-383, Gif-sur-Yvette, France, 1995, Ed. B. Bonin.

[10] Y. Kijima et al., Proc. of 10^{th} Workshop on RF Superconductivity, 2001 & Proc. of EPAC 2000, Vienna, Austria.

[11] Y. Tuckmantel et al., Proc. of the 1995 Particle Accelerator Conference, Dallas, USA.

[12] Y. Morita et al., Presented at the 11^{th} Workshop on RF Superconductivity, Lubeck, Germany 2003.

[13] E. Chojnacki, Phys. Rev. ST AB. 3, 032001 (2000).

[14] G. Devanz, Phys. Rev. STAB. 4, 012001 (2001).

[15] R.L. Geng, H. Padamsee & V. Shemelin, Presented at the 2001 Particle Accelerator Conference, Chicago, USA, June 18-22, 2001.

[16] E. Somersalo, P. Yla-Oijala, D. Proch and J. Sarvas, Part. Accl. 61, 107 (1998).

[17] V. Baglin et al., Proc. of EPAC 2000, Vienna, Austria, p.217-221.

[18] R. Calder et al., Nucl. Inst. Meth. B13, 631 (1986).

[19] R. Noer et al., Proc. of 10^{th} Workshop on RF Superconductivity, Tsukuba, Japan 2001.

[20] H. Padamsee and A. Joshi, J. Appl. Phys. 50, 1112, (1979).

[21] A. G. Mathewson, CERN AT/92-33 (VA).

[22] Y. Bozhko and H. Hillert, AT-VAC CRN1995